Tectonophysics 626 (2014) 170–185

Contents lists available at ScienceDirect

Tectonophysics

journal homepage: www.elsevier.com/locate/tecto

Vestiges of the proto-Caribbean seaway: Origin of the San Souci Volcanic Group, Trinidad

Iain Neill [a,*], Andrew C. Kerr [a], Kevin R. Chamberlain [b], Axel K. Schmitt [c], Franco Urbani [d], Alan R. Hastie [e], James L. Pindell [a,f], Tiffany L. Barry [g], Ian L. Millar [h]

[a] School of Earth and Ocean Sciences, Cardiff University, CF10 3AT, UK
[b] Department of Geology and Geophysics, University of WY, Laramie, 82071-3006, USA
[c] Department of Earth, Planetary, and Space Sciences, University of CA Los Angeles, 90095-1567, USA
[d] Fundación Venezolana de Investigaciones Sismológicas & Universidad Central de Venezuela, Dept. de Geología, Caracas, Venezuela
[e] School of Geography, Earth and Environmental Sciences, University of Birmingham, B15 2TT, UK
[f] Tectonic Analysis, Ltd., Chestnut House, Burton Park, Duncton, GU28 0LH, UK
[g] Department of Geology, University of Leicester, LE1 7RH, UK
[h] NERC Isotope Geosciences Laboratory, Keyworth, Nottingham, NG12 5GG, UK

ARTICLE INFO

Article history:
Received 4 February 2014
Received in revised form 1 April 2014
Accepted 8 April 2014
Available online 22 April 2014

Keywords:
Caribbean
Geochemistry
Ion microprobe
Tectonics
Zircon

ABSTRACT

Outcrops of volcanic–hypabyssal rocks in Trinidad document the opening of the proto-Caribbean seaway during Jurassic–Cretaceous break-up of the Americas. The San Souci Group on the northern coast of Trinidad comprises the San Souci Volcanic Formation (SSVF) and passive margin sediments of the ~130–125 Ma Toco Formation. The Group was trapped at the leading edge of the Pacific-derived Caribbean Plate during the Cretaceous–Palaeogene, colliding with the para-autochthonous margin of Trinidad during the Oligocene–Miocene. In-situ U–Pb ion probe dating of micro-zircons from a mafic volcanic breccia reveal the SSVF crystallised at 135.0 ± 7.3 Ma. The age of the SSVF is within error of the age of the Toco Formation. Assuming a conformable contact, geodynamic models indicate a likely origin for the SSVF on the passive margin close to the northern tip of South America. Immobile element and Nd–Hf radiogenic isotope signatures of the mafic rocks indicate the SSVF was formed by ≪10% partial melting of a heterogeneous spinel peridotite source with no subduction or continental lithospheric mantle component. Felsic breccias within the SSVF are more enriched in incompatible elements, with isotope signatures that are less radiogenic than the mafic rocks of the SSVF. The felsic rocks may be derived from re-melting of mafic crust. Although geochemical comparisons are drawn here with proto-Caribbean igneous outcrops in Venezuela and elsewhere in the Caribbean more work is needed to elucidate the development of the proto-Caribbean seaway and its rifted margins. In particular, ion probe dating of micro-zircons may yield valuable insights into magmatism and metamorphism in the Caribbean, and in altered basaltic terranes more generally.

1. Introduction

Rifting of the supercontinent Pangaea and the opening of the Central Atlantic during the Mesozoic represents both a classic example of continental break-up and passive margin development, and an enduring enigma in assessing the role of mantle plumes in such a process (e.g., Callegaro et al., 2013; Hill, 1993; McHone, 2000). One branch of the Pangaea break-up story that has hitherto received little attention is the rifting of North and South America from the latest Triassic onwards (e.g., Bartok, 1993; Ostos et al., 2005). This rifting generated both the Gulf of Mexico and the proto-Caribbean seaway (Pindell and Dewey, 1982), and lasted until the onset of N–S convergence between the Americas in the Late Cretaceous (Müller et al., 1999). The Pacific-derived Caribbean Plate has over-ridden much of the proto-Caribbean since the Cretaceous. Only fragments of proto-Caribbean crust which have been either accreted to the Caribbean Plate or thrust onto South America remain, from which the tectono-magmatic evolution of the proto-Caribbean oceanic crust have to be pieced together. Many of these 'fragments' in South America have hitherto received little attention.

During the Late Jurassic–Early Cretaceous, the proto-Caribbean seaway was fringed on its western margin by east-dipping subduction of the Farallon Plate, generating the 'inter-American Arc' (e.g., Pindell and Dewey, 1982). During the Early–Late Cretaceous (see Hastie and Kerr, 2010; Pindell et al., 2011; Hastie et al., 2013; Escuder Viruete

* Corresponding author at: Department of Earth Sciences, University of Durham, DH1 3LE, UK. Tel.: +44 1913 342356.
E-mail address: iain.neill@durham.ac.uk (I. Neill).

http://dx.doi.org/10.1016/j.tecto.2014.04.019

et al., 2014, for recent debate), east-dipping subduction beneath the inter-American Arc ceased and was superseded by SW-dipping subduction of proto-Caribbean oceanic crust. Proto-Caribbean subduction gave rise to the 'Great Arc of the Caribbean' (sensu Burke, 1988), a composite of several island arc systems of debated origin and complexity (Neill et al., 2011; Wright and Wyld, 2011). This arc system includes much of the present-day Greater Antilles, Aves Ridge, and Netherlands-Venezuelan Antilles as well as Tobago and allocthonous terranes in Venezuela, and marked the leading edge of the Pacific-derived Caribbean Plate from the Cretaceous to the Palaeocene. These subduction systems shut down following roll-back of the proto-Caribbean slab and were superseded by growth of the Palaeocene–Eocene to present-day Lesser Antilles Arc system.

The central region of the Caribbean Plate consists of 7–20 km thick crust of the Late Cretaceous mantle plume-derived Caribbean Oceanic Plateau (see review in Kerr et al., 2003). Due to continued Atlantic spreading and Andean–Cordilleran subduction, the Pacific-derived Caribbean Plate has moved east relative to the Americas from the Cretaceous to the present, with much of the proto-Caribbean oceanic crust being subducted beneath the 'Great Arc' system. Therefore, models of how and when North and South America broke apart remain to be tested properly, and the role of igneous processes in continental break-up in this region is still uncertain as we have little proto-Caribbean crust to work with.

Fortunately, a few fragments of Mesozoic proto-Caribbean crust and lithospheric mantle escaped subduction, having been either accreted to the present-day Greater or Lesser Antilles (e.g., Jolly et al., 2008; Marchesi et al., 2011; Neill et al., 2010) or been thrust onto northern South America (Kerr et al., 2009; Ostos and Sisson, 2005; Wadge and Macdonald, 1985) (Fig. 1). Nevertheless, a further problem remains in studying such proto-Caribbean outcrops in that many of these contain altered mafic rocks which are inherently difficult to interpret geochemically and to date accurately due to mobilisation of major and trace elements. In this paper, we present new ion microprobe U–Pb zircon geochronology along with immobile element and Nd–Hf radiogenic isotope data from the San Souci Volcanic Formation of northeast Trinidad (Fig. 2), the easternmost exposure of igneous rocks on the Caribbean coast of South America. We use the new data to re-assess the timing and source of magmatism at San Souci and its relationship to both the break-up of the Americas and later Caribbean tectonics. Furthermore, this work demonstrates the potential for accurate dating of altered fine-grained Phanerozoic mafic rocks.

2. Geological setting and studied samples

2.1. The Caribbean–South American Plate boundary

Northern South America is a tectonically complex transpressive plate boundary between the Caribbean and South American Plates. South America is currently moving to the west at ~20 mm a^{-1} relative to the Caribbean Plate, with much of the motion taken up on the El Pilar–San Sebastian fault system running through Trinidad and Venezuela (Weber et al., 2001) and the offshore North Coast Fault Zone to the north of Trinidad (Figs. 1,2). In pre-Cenozoic times, northern South America was a passive margin of the proto-Caribbean seaway between North and South America, with the future

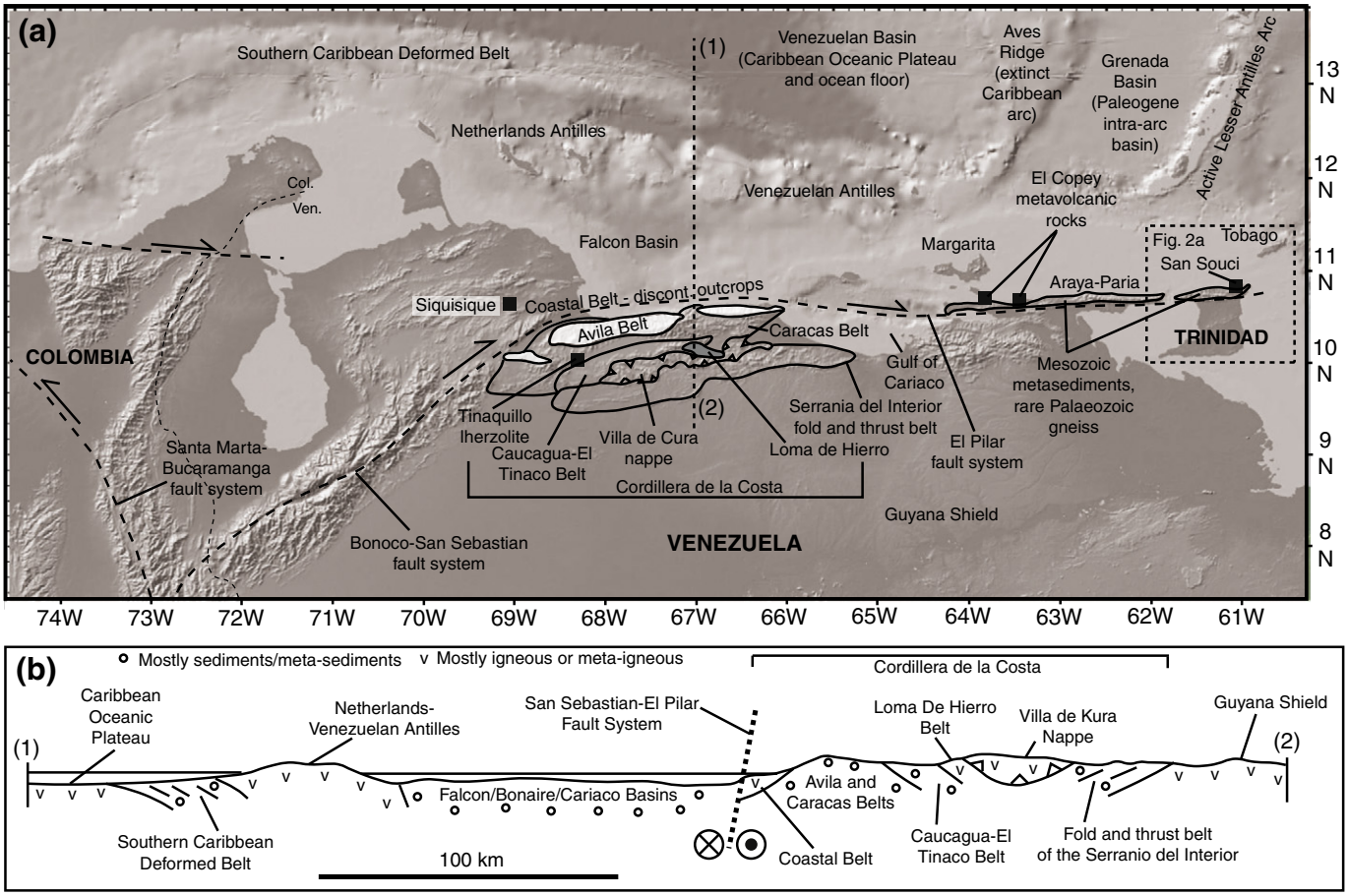

Fig. 1. (a) Map of the Caribbean–South American Plate boundary region showing the units mentioned in the text. Geological units adapted from Urbani and Rodríguez (2004) and Hackley et al. (2005). Background topography map is from www.geomapapp.org (Haxby et al., 2010; Ryan et al., 2009). (b) Geological cross section from north to south through the Caribbean–South American Plate boundary at around 67°W modified from Giunta et al. (2002).

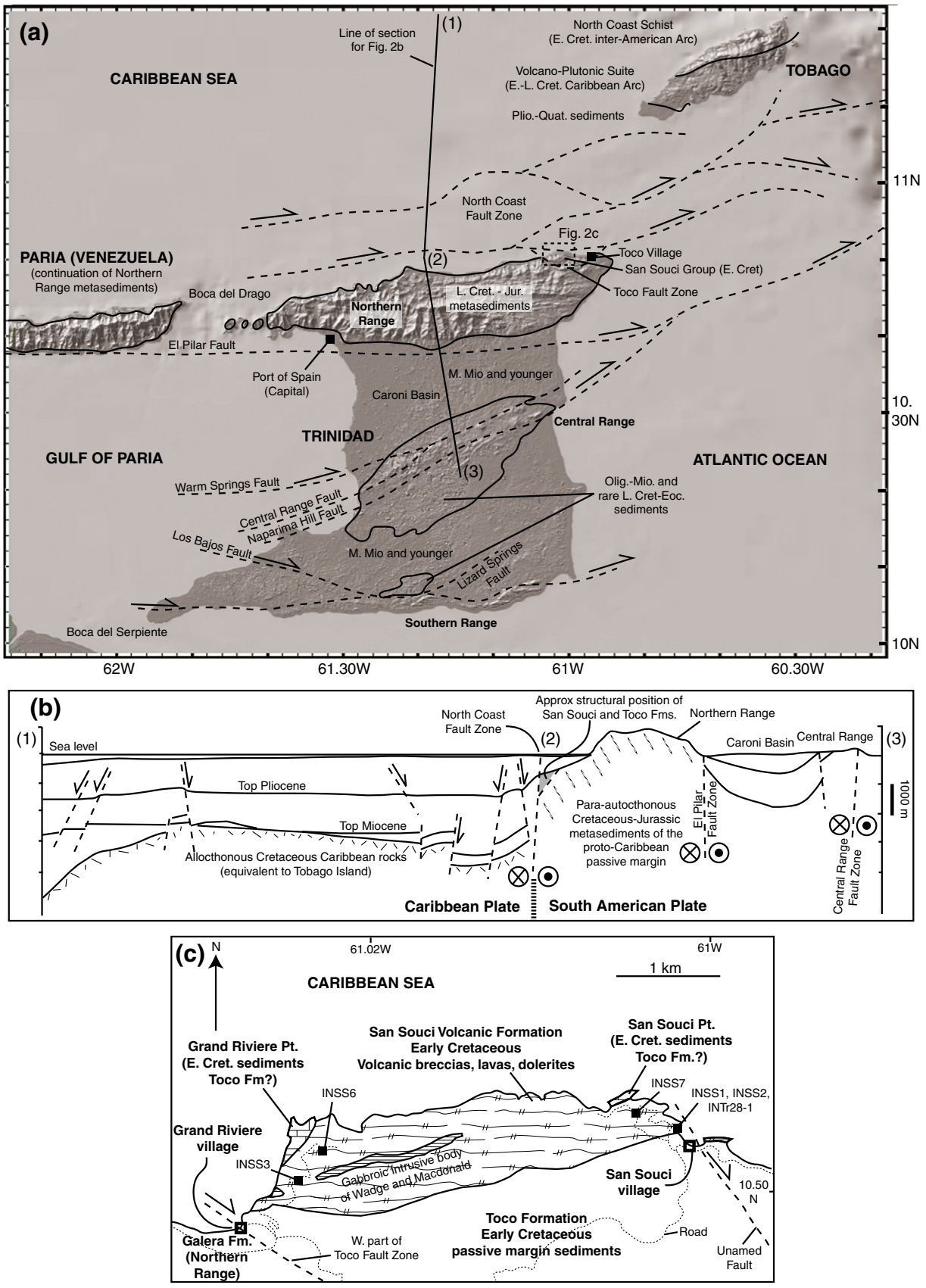

Fig. 2. (a) Geological map of the Trinidad and Tobago region showing major geological units and strike–slip fault systems. simplified from Robertson and Burke (1989), Algar (1998) and Snoke et al. (2001b), with topography from www.geomapapp.org (Haxby et al., 2010; Ryan et al., 2009). (b) Cross-section modified from Robertson and Burke (1989) through the North Coast Fault Zone and northern Trinidad, showing equivalent position of San Souci which lies to the east of the section. (c) Sample location map for San Souci and the Toco Formation after Wadge and Macdonald (1985).

Caribbean region lying in the Pacific to the west of South America as part of the Farallon Plate (Maresch, 1974). After inception of southwest-dipping subduction beneath the Great Arc, the Caribbean Plate advanced north-eastwards relative to the Americas, consuming proto-Caribbean oceanic crust. Tectono-stratigraphic data reveal that the leading edge of the Caribbean Plate began to interact with northwest South America by ~75 Ma (Vallejo et al., 2006; Weber et al., 2010). The Caribbean Plate then collided with the South American passive margin diachronously from west to east during the Cenozoic, generating mountainous terrain such as the Cordillera de la Costa in Venezuela and the Northern Range of Trinidad (Escalona and Mann, 2010; Pindell and Barrett, 1990) (Fig. 1).

2.2. The Caribbean–South American Plate boundary zone in Venezuela

The present diffuse plate boundary in central Venezuela is divided from north to south into five crustal units (Fig. 1a,b): (1) The most northerly unit is the Southern Caribbean Deformed Belt, a sub-sea wedge of S-dipping sedimentary rocks (Bezada et al., 2010). (2) Next are the Netherlands-Venezuelan Antilles, fragments of Caribbean Oceanic Plateau and island arc rocks (see Kerr et al., 1996; Loewen et al., 2013; Wright and Wyld, 2011). (3) Third is the Falcon Basin, a series of pull-apart basins filled with Neogene sediments (Muessig, 1984). (4) The fourth unit is the Cordillera de la Costa, which is subdivided into six belts (Urbani and Rodríguez, 2004), as: (a) the Coastal Belt, a fringe of Mesozoic rocks characterised by high pressure-low temperature (HPLT) mineral assemblages (Sisson et al., 1997); (b) the Ávila Belt consisting of Paleozoic continental rocks, meta-sediments and meta-granitoids; (c) the Caracas Belt with Mesozoic passive margin sediments; (d) the Caucagua–El Tinaco Belt, containing Neoproterozoic to Eocene continental material; (e) the Loma de Hierro Belt, which is likely to be an ophiolite of proto-Caribbean origin affected by low grade metamorphism (see discussion in Section 6.1); and (f) the Villa de Cura Belt, a klippe which has overridden the passive margin units of northern South America (Maresch, 1974). The latter is divided into two terranes, the Villa de Cura sensu stricto with HPLT assemblages belonging to an island arc-related subduction complex, and the unsubducted San Sebastian Terrane which reaches prehnite–pumpellyite facies only. The rocks of the Villa de Cura Belt are probably fragments of the inter-American or 'Great Arc' and may correlate with rocks found on Margarita and Tobago Islands to the east (Maresch et al., 2009; Neill et al., 2012; Snoke et al., 2001a). (5) Finally, the fold-and-thrust belt of the Serranía del Interior containing para-autochthonous sedimentary rocks is the most southerly unit affected by Caribbean–South American Plate interaction (Hung, 2005).

In northeastern Venezuela, the belts described from the Cordillera de la Costa largely disappear beneath the Gulf of Cariaco (Fig. 1a) and are replaced in the Araya–Paria region primarily by Mesozoic meta-sedimentary rocks from the proto-Caribbean passive margin (Hackley et al., 2005). There are also 2 km-scale exposures of Palaeozoic gneiss (Hackley et al., 2005), suggesting that much of the Araya–Paria region may be broadly equivalent to the Ávila or Caucagua–El Tinaco Belts. On the very northern coast of the Araya Peninsula, there are meta-tuffs, pillow basalts and serpentinites known as the El Copey Meta-volcanic Formation (McMahon, 2000; Seijas, 1971) (Fig. 1a). These are discussed in Section 6.1 and are considered to be of proto-Caribbean origin.

2.3. The Caribbean–South American Plate boundary zone in Trinidad

Trinidad, unlike Venezuela, comprises relatively few igneous and meta-igneous rocks. Much of the island developed para-autochthonously on the Mesozoic to Early Cenozoic passive margin of the proto-Caribbean Seaway (Algar, 1998). Exceptions are altered tholeiitic tuff horizons in the Barremian (~130–125 Ma) Maracas Formation of the Northern Range (Jackson et al., 1991) and the San Souci Volcanic Formation (Wadge and Macdonald, 1985). Trinidad has mountainous terrain to the north of the island (the Northern Range, reaching up to 1 km above sea level) and basins (e.g., the Caroni Basin) and low hills of a few hundred metres elevation (the Central and Southern Ranges) to the south. The island is cut by successive right-lateral strike–slip fault systems (Fig. 2a, Algar, 1998). The El Pilar Fault (Fig. 2a,b) cuts the southern edge of the Northern Range and roughly marks the boundary between non-metamorphic facies and the metamorphic rocks of the Northern Range. The Northern Range consists mostly of Jurassic to Upper Cretaceous proto-Caribbean passive margin protoliths (Algar, 1998). The Range underwent Oligocene–Miocene greenschist–facies metamorphism and penetrative deformation co-incident with collision between the Caribbean Plate and the passive margin (Algar and Pindell, 1991, 1993; Speed and Foland, 1991).

2.4. The San Souci Group[1]: San Souci Volcanic Formation and Toco Formation

The San Souci Group (Algar and Pindell, 1991) lies in an isolated location on the northern coast of Trinidad, between the villages of Toco and Grand Riviere (Fig. 2a,c) and is not geologically part of the Northern Range. The Group consists of both sedimentary and igneous rocks. The Caribbean 'Great Arc' rocks of Tobago Island (Snoke et al., 2001a) are 35 km to the north, whilst the Toco–Grand Riviere fault system separates the San Souci Group from the Northern Range meta-sediments (Algar and Pindell, 1993) to the south. The Toco–Grand Riviere fault system is a splay from the offshore North Coast Fault Zone, marking the effective Caribbean–South American Plate boundary (Robertson and Burke, 1989) (Fig. 2b). The San Souci Group consists of the San Souci Volcanic Formation (SSVF), dominated by mafic sub-aerial volcanic and hypabyssal rocks (described in more detail in Section 2.5), and the Toco Formation which contains fine black shales and interdigitated coarse quartzo-feldspathic sandstone channels along with calcareous shales, grits and thin limestone bands (Barr, 1962; Wadge and Macdonald, 1985). Exposure is severely limited by tropical weathering and jungle vegetation.

The San Souci Group only reaches prehnite–pumpellyite facies and does not show penetrative deformation. The oldest zircon fission track ages from the Toco Formation range from the Permian to Early Jurassic, coinciding with ages of granitoids in western Venezuela and Colombia (Algar et al., 1998). The Toco Formation was thus likely deposited on the proto-Caribbean margin of South America, but was then transported eastward relative to South America after accretion to the leading edge of the Caribbean Plate. During fieldwork, the contact between the SSVF and the Toco Formation was not exposed.

Barr (1962, 1963) identified solitary and colonial coral, bivalve, echinoderm, ammonoid and foraminiferal assemblages within calcareous shale and limestone units of the Toco Formation, including the ammonite *Pulchellia*, which is of Barremian age (130–125 Ma). However, the youngest zircon fission track ages obtained from two sandstone samples cluster at ~108 Ma (Albian) (Algar et al., 1998). The ages were proposed to represent detritus from the 'Great Arc' or the then-undated SSVF (Algar and Pindell, 1993; Algar et al., 1998), implying an Albian age for part of the Toco Formation (incompatible with the faunal ages), and/or a similar age for the SSVF. On the basis of our geochronological and isotope geochemistry results we can rule out both these possibilities and instead propose that the ~108 Ma ages represent uplift following a prehnite–pumpellyite facies metamorphic event which partially annealed Toco Formation zircons. Wadge and Macdonald (1985) obtained a K–Ar age of 87 ± 4.4 Ma from a basalt of the SSVF at San Souci Point (Fig. 1b) but this age is questionable given extensive hydrothermal alteration of the SSVF.

Limited geochemical data (Wadge and Macdonald, 1985) have precluded detailed petrogenetic assessment of the SSVF. Previous

[1] *Both 'Sans Souci' (Fr. 'carefree') and 'San Souci' are used in the literature. We use the latter in direct reference to the village of the same spelling within the field area.*

interpretations of the origin of the SSVF range from proto-Caribbean MORB (Algar and Pindell, 1993) or a seamount (Algar, 1993) to an outlier of the Caribbean Oceanic Plateau (Kerr et al., 2003; Wadge and Macdonald, 1985).

2.5. Petrography of studied samples

The SSVF is dominated by massive sub-aerial mafic volcanic rocks, thought to have been auto-brecciated by repeated magmatism (Wadge and Macdonald, 1985) and perhaps also affected by interaction with sea-water, although the lack of altered glass indicates these are not hyaloclastites. Also present are hypabyssal dolerites which appear to intrude the volcanic pile. A 100 m-wide dyke-like dolerite body is said to lie in a fault-bounded unit 6 km to the south-east of San Souci, and a gabbro-dolerite intrusion was noted from the middle of the formation by Wadge and Macdonald (1985), but neither were exposed during fieldwork for this study due to dense vegetation. The freshest available samples of the least brecciated and altered extrusive and intrusive rocks were collected from track cuttings near Grand Riviere and from cuttings and shoreline at San Souci Point (Fig. 2c). The coarser rocks of the SSVF are aphyric dolerites, of 1–2 mm grain size, with a primary mineralogy of interlocking elongate plagioclase and clinopyroxene. The finer-grained mafic auto-breccias contain elongate, randomly-aligned plagioclase and stubby clinopyroxene. All rocks have undergone alteration: plagioclase is partially replaced by clays and sericite, and veins and small alteration patches contain assemblages dominated by chlorite, with prehnite, pumpellyite, clays, calcite, epidote, and Fe–Ti oxides.

During this study an outcrop of uncertain stratigraphic position was discovered in a recent quarry towards the eastern end of the SSVF (Sample location 7 on Fig. 2c). This outcrop consists of felsic plagioclase-phyric auto-breccias with elongate to needle-like groundmass plagioclase, quartz, squat clinopyroxene often altered to chlorite, and Fe–Ti oxides. These felsic samples also contain some quartz-calcite veining. A single sample from the Toco Formation was also collected, an impure sandstone containing very fine angular quartz (~65%, approximately 0.25 mm grain size), heavily altered calcified feldspar grains and some platy muscovite (<5%).

3. In-situ geochronology of the SSVF

3.1. Methodology and textural information

Glass or mineral separates from fine-medium grained mafic igneous rocks are normally dated by Ar–Ar methods. An earlier attempt to date plagioclase crystals was unsuccessful owing to the degree of alteration. Analysis was instead undertaken on zircons and baddeleyites found in the SSVF following protocols outlined for the analysis of small (<50 μm) grains using the secondary ion microprobe (SIMS) on thick-sectioned samples (Chamberlain et al., 2010; Schmitt et al., 2010). Baddeleyite (ZrO_2) is an accessory mineral in mafic igneous rocks (Krogh et al., 1987), whilst zircon replaces baddeleyite during magmatic evolution and low-grade metamorphism as well as being a primary magmatic phase (Heaman and LeCheminant, 1993). Sample INSS6.3 was selected for analysis, an aphyric brecciated dolerite with approximately 1 mm grain size. A thick section of sample INSS6.3 was imaged using reflected light then mapped using a JEOL JXA8900 electron microprobe at the University of Wyoming to find high-Zr phases, most of which were between 5 and 30 μm in diameter. Back-scatter imaging was then used for identification. The section contained isolated grains of baddeleyite with minimal rims of zircon, at least as many mixed grains with a core of baddeleyite and a mantle of zircon, plus numerous zircons, either misshapen or euhedral, which lack baddeleyite entirely. Examples of these textures are found in Supplementary Item A. Textural analysis allows identification of grains which are unsuitable for analysis. U–Pb ages are calculated assuming the crystal is solely one phase or the other, so mixed grains are rejected. Finally, the distinct populations of zircon are interpreted differently: misshapen zircons are probably late overgrowths entirely replacing baddeleyite, whereas euhedral zircons are considered to be magmatic.

Baddeleyites and zircons selected for dating were analysed on the Cameca IMS 1270 SIMS instrument at the University of California, Los Angeles in two runs during 2011 and 2012. An aperture in the transfer section of the secondary beam column was used to reduce the effective sampling diameter from ~20 μm to ~8 μm. In line with previous protocol, the sample chamber was flooded with oxygen (~3×10^{-5} Torr for zircon,~1×10^{-5} Torr for baddeleyite) to enhance recovery of secondary ions of Pb approximately 10-fold (e.g., Schuhmacher et al., 1993; Wingate and Compston, 2000). U/Pb relative sensitivity was calibrated using UO_2/U for baddeleyite using the Phalaborwa standard and using UO/U for zircon using standard AS3. UO_2/U ranged from 6.2 to 7.0 (2011 run) whilst UO/U ranged from 7.9–8.3 (2011) to 6.52–8.52 (2012). Pb values were corrected for common Pb using ^{204}Pb for both baddeleyite and zircon.

3.2. Zircon U–Pb results

Results are presented in Table 1 and graphically in Supplementary Items B1 and B2. Of the dateable grains, 11 zircons give a $^{206}Pb/^{238}U$ weighted mean age of 135.0 ± 7.3 Ma. Misshapen zircons taken to be replacing baddeleyite and euhedral zircons have ages within error of one other, indicating that the baddeleyite-zircon transformation likely occurred during crystallisation. A single baddeleyite grain (not included in the weighted mean) gave an age close to being within error of the other ages (Table 1). As baddeleyite cannot be generated by low-grade metamorphic processes, this age strongly supports the magmatic origin of the zircon population.

4. Whole-rock geochemistry

4.1. Analytical methods

Whole rock samples were prepared and analysed for major and trace elements at Cardiff University using methods outlined in McDonald and Viljoen (2006). Samples were powdered by agate ball mill and after determination of loss on ignition (900 °C for 2 h) were fused on a propane burner with $LiBO_2$ in platinum crucibles, and dissolved in HNO_3. Analysis by inductively coupled plasma optical emission spectrometry (ICP-OES) was undertaken for major elements and Sc using a JY-Horiba Ultima 2 instrument. Mass spectrometric (ICP-MS) trace element analysis was carried out using a Thermo Elemental X7 Series for minor, trace and rare earth elements (REE). International mafic rock standards including JB-1A and BIR-1 were run at regular intervals throughout the analysis time. Precision for most major elements during standard runs were better than 2.7% (except P_2O_5 = 5.8%), and better than 3% for most trace elements, excepting 5.1% for Ni, 4.1% for Cu, 7.6% for Rb (1σ). Standard deviations were always better than 4.7% for the REE (1σ). Results are presented in Table 2, including data produced for mafic rocks at El Copey and Siquisique in Venezuela for Kerr et al. (2009) (see Section 6.1). Standard runs are in Supplementary Item C.

Nd–Hf radiogenic isotope analyses were undertaken at NIGL in Nottingham, UK, by dissolution of non-ignited samples using a standard HF-HNO_3 digestion technique. Hf was obtained using the LN-SPEC column separation method (Münker et al., 2001), and samples were analysed on a Nu-plasma multicollector ICP-MS. Reverse mass-bias correction with empirically determined $^{176}Yb/^{173}Yb$ and $^{176}Lu/^{175}Lu$ ratios was employed, although separation techniques ensured samples contained little Yb and no Lu was present. Results for standards (JMC475: $^{176}Hf/^{177}Hf = 0.282161 \pm 0.000006$ at 1σ, n = 45, 2σ analytical uncertainty = 45 ppm; BCR2: $^{176}Hf/^{177}Hf = 0.282866 \pm 0.000006$ at 1σ, n = 7, 2σ analytical uncertainty = 40 ppm) were comparable to preferred values of 0.282160 for JMC475 (Nowell and

Table 1
SIMS data from in-situ analyses of zircon and baddeleyite in sample INSS6.3, San Souci Volcanic Formation.

Grain	Description	Size (μm)	Ages (Ma)					Ratios							Run
			$^{206}Pb/^{238}U$	±1 s.e.	r^{206}Pb %	U ppm	Th/U$^{\$}$	$^{207}Pb^{*}/^{235}U$	1 s.e. %	$^{206}Pb^{*}/^{238}U$	1 s.e. %	rho	UO_2/U	UO/U	
Zircon			Weighted mean $^{206}Pb/^{238}U$ zircon date = 135.0 ± 7.3 Ma (2σ) (MSWD 1.4)												
18z	bd rep	20 × 8	175	14	97.7	621	2.6068	0.165	43	0.0274	8	0.422		7.8	03/03/2011
25z	bd rep	28 × 10	162	12	98.9	741	2.3079	0.184	24	0.0254	8	0.458		7.9	03/03/2011
21z	euhedral	25 × 5	145	11	100.0	739	2.07074	0.175	30	0.0227	7	0.457		8.1	03/03/2011
22z	bd rep	22 × 10	145	9	98.4	772	2.74694	0.168	39	0.0227	7	0.474		8.6	03/03/2011
6z	euhedral	22 × 18	141	8	103.0	469	1.9976	0.334	14	0.0221	5	0.570		8.3	24/01/2012
19z	euhedral	18 × 8	138	10	99.3	754	0.99078	0.138	15	0.0216	8	0.552		7.9	03/03/2011
3z	bd rep	30 × 8	137	7	92.0	769	1.2496	0.131	16	0.0215	6	0.430		8.1	24/01/2012
17z	euhedral	22 × 10	134	9	99.0	1159	3.83572	0.123	37	0.0209	7	0.400		8.0	03/03/2011
10z	bd rep	50 × 10	126	9	98.6	641	2.2176	0.166	26	0.0197	7	0.470		7.5	24/01/2012
4z	bd rep	18 × 6	125	7	86.0	658	1.5928	0.265	27	0.0196	5	0.550		9.3	24/01/2012
2z	bd rep	15 × 5	125	8	100.0	844	2.464	0.224	32	0.0195	6	0.640		8.3	24/01/2012
Baddeleyite			Baddeleyite grain not included in final date												
24bd	thin z rim	12 × 8	155	8	93.8	545	0.93492	0.056	81	0.0244	5	0.355	5.3		03/03/2011

Notes: values in parentheses are absolute errors at one sigma level for ages, percent for ratios.
bd = baddeleyite, z = zircon, rep = zircon replacing bd.
r^{206}Pb = radiogenic ^{206}Pb in percent.
$ = SIMS ThO/UO data converted to atomic Th/U.
* = radiogenic Pb value corrected for initial Pb using ^{204}Pb method for both baddeleyite and zircon.
rho = correlation coefficient of error ellipses.

Parrish, 2001) and 0.282879 for BCR2 (Blichert-Toft, 2001), so no corrections were made. Light rare earth elements (LREE) were concentrated on Eichrom AG50 cation columns, and analysed using a Thermo Scientific Triton TIMS machine in multi-dynamic mode. The $^{143}Nd/^{144}Nd$ results for the La Jolla standard were: 0.511846 ± 0.000003 at 1σ (n = 6, 2σ analytical uncertainty = 12 ppm). Here, results are normalised to a preferred value of $^{143}Nd/^{144}Nd$ = 0.511860. Isotope results are presented in Table 3, along with results for El Copey and Siquisique (Section 6.1) produced for Kerr et al. (2009).

4.2. Mafic rocks

Hydrothermal alteration, low-grade metamorphism and weathering mean that fluid-mobile major and large ion lithophile element (LILE) concentrations are not likely to be representative of the original SSVF magma, whereas Th, REE, transition metals and High Field Strength Elements (HFSE) are relatively immobile under such conditions (Cann, 1970). Therefore we will focus on these immobile elements in furthering our assessment of the petrogenesis of the SSVF. The Th vs. Co and Zr/Ti vs. Nb/Y classification diagrams designed for such altered rocks (Hastie et al., 2007; Pearce, 1996) indicate that the majority of SSVF mafic rocks are tholeiitic basalts and basaltic andesites, with just 3 samples classified as calc-alkaline basaltic andesites (Fig. 3a, b).

San Souci samples contain ~46–56 wt.% SiO_2 and <8 wt.% MgO (Mg# = 55–66), indicating that they are not primary magmas (Fig. 3c and e, Table 2). Immobile, incompatible element variation diagrams such as TiO_2 vs. Yb (Fig. 3d) show that most samples lie on a broad trend, and might therefore be related to each other by fractional crystallisation, although a single sample lies off-trend and may be representative of a distinct magmatic suite. Chondrite-normalised REE diagrams have relatively flat patterns (10–30 times chondrite), with slight LREE/HREE (light/heavy REE) enrichment (La_{CN}/Yb_{CN} = 0.9–2.3) (Fig. 4a). Small Eu anomalies may be ascribed to plagioclase fractionation or accumulation. The primitive mantle-normalised trace element patterns for the rocks (Fig. 4b) have conspicuous negative Th anomalies along with relatively small positive Nb–Ta and Zr–Hf anomalies. The LREE-enriched samples have more conspicuous positive Nb–Ta anomalies. The most evolved mafic samples have negative Ti anomalies.

4.3. Felsic rocks

The two felsic samples (SS7.1 and 7.3) plot as a calc-alkaline andesite/dacite and shoshonitic dacite respectively on a Th–Co discrimination diagram (Fig. 3a) or as trachy-andesite/phonolite on a Zr/Ti vs. Nb/Y plot (Fig. 3b). They have lower Fe_2O_3, TiO_2, MgO and CaO and higher Al_2O_3 and Na_2O compared to the mafic rocks (Table 2). The trace element contents are also distinct, with very high HFSE concentrations and much lower Ni and Cr compared to the mafic samples (Table 2). These felsic rocks have concave chondrite-normalised REE patterns with high LREE/MREE (middle REE) ratios (Fig. 4c). The samples have no depletion in the HREE and appear to lack Eu anomalies. On a primitive mantle-normalised trace element plot (Fig. 4d), the felsic rocks have large negative Ti anomalies and very large positive Zr–Hf and Nb–Ta anomalies with moderate Nb/Ta (~15) but very high Zr/Hf (55). Th is slightly enriched over the LREE.

The single sandstone from the adjacent Toco Formation has ~81 wt.% SiO_2 and low concentrations of Al_2O_3 and K_2O (Table 2) probably derived from muscovite, altered feldspar and clays. For the most part, the sandstone has identical REE and normalised trace element patterns to the felsic volcanic rocks, with the exception of a very large negative Nb–Ta anomaly on the primitive mantle-normalised plot (Fig. 4d). This discrepancy suggests that the volcanic and sedimentary rocks are genetically unrelated.

4.4. Radiogenic isotopes

Isotopic ratios of the mafic rocks of the SSVF vary little, and are more radiogenic than Bulk Earth, with initial values at 135 Ma of εHf ~ 13.9 and εNd ~ 8.9 (Fig. 5, Table 3). The two felsic samples from San Souci, also corrected to initial values at 135 Ma in the absence of better age constraints, are less radiogenic than the mafic rocks, with εHf of ~9.7 and εNd of ~6.1. The Toco Formation sandstone has isotopic signatures typical of mature continental crust (εHf = −23, εNd = −14) so is not plotted on Fig. 5. There is clearly no connection between the SSVF and the Toco Formation, nor does the Toco Formation have isotopic signatures consistent with Caribbean Great Arc input (cf. the ~110–105 Ma Tobago Volcanic Group; Neill et al., 2013).

Table 2
Major and trace element data for the San Souci Volcanic Formation, plus results from Kerr et al. (2009) for the El Copey and Siquisique localities discussed in the text. LOI—loss on ignition. D = dolerite, B = breccia in sample names. bd = below detection.

Unit	San Souci Volcanic Formation—mafic rocks															
Sample	28-1/1	INSS3a1	INSS3a2	INSS3b1	INSS3b2	INSS3cD	INSS3cB	INSS3d	INSS3e	INSS3f	INSS6.1	INSS6.2	INSS6.3	INSS6.4	INSS6.5	INSS7.2
SiO_2	50.86	45.60	47.47	50.11	47.86	49.34	52.89	50.66	48.15	48.64	51.01	49.92	50.90	48.79	56.21	51.07
TiO_2	1.84	1.47	1.69	1.31	1.54	1.63	1.30	0.99	1.92	1.69	1.91	1.20	1.55	1.97	1.18	1.24
Al_2O_3	14.19	14.77	14.35	15.53	14.30	14.46	13.96	13.92	14.43	14.21	12.98	13.95	14.11	13.88	14.09	15.08
Fe_2O_3(T)	10.05	9.48	10.57	9.02	8.60	9.06	8.12	7.93	11.65	11.77	10.56	9.02	9.44	11.00	6.48	8.78
MnO	0.14	0.17	0.14	0.16	0.14	0.15	0.12	0.12	0.18	0.18	0.14	0.16	0.16	0.18	0.12	0.17
MgO	6.40	6.69	7.62	7.30	5.84	6.05	7.83	7.80	7.20	8.18	6.20	7.00	6.68	6.76	4.22	7.85
CaO	6.54	8.16	6.26	8.26	7.98	6.46	7.91	9.83	9.02	8.86	9.49	11.26	9.57	9.96	8.91	10.74
Na_2O	5.29	4.32	3.63	4.27	4.54	4.37	4.70	4.71	3.50	3.13	3.29	3.35	4.38	3.77	5.13	3.66
K_2O	0.16	0.19	0.13	0.15	0.09	0.13	0.34	0.39	0.09	0.09	0.03	0.16	0.14	0.04	0.13	0.12
P_2O_5	0.24	0.16	0.16	0.12	0.17	0.16	0.19	0.10	0.21	0.16	0.23	0.14	0.15	0.21	0.17	0.13
LOI	3.01	9.88	9.10	3.56	9.66	8.85	2.69	3.97	3.42	3.76	3.04	2.77	2.46	2.89	2.47	2.82
Total	98.71	100.90	101.12	99.79	100.72	100.65	100.05	100.42	99.78	100.68	98.89	98.93	99.55	99.44	99.13	101.65
Sc	33.3	32.4	37.0	35.0	31.0	31.3	33.2	28.6	40.4	38.3	37.4	35.5	34.1	37.5	32.1	34.1
V	260.3	276.6	318.7	253.9	274.9	289.6	256.2	208.1	341.1	310.0	306.0	237.5	264.5	323.8	201.2	238.2
Cr	208.8	180.3	217.9	294.7	167.8	182.1	238.1	283.3	106.4	156.7	98.3	174.7	149.9	155.4	129.8	343.8
Co	31.1	34.8	36.2	34.6	31.6	32.7	31.2	32.5	37.3	39.4	35.8	31.8	31.8	37.9	20.1	33.8
Ni	101.6	81.8	59.9	81.8	72.9	69.2	82.1	96.8	51.7	65.9	48.0	65.8	86.6	54.0	37.4	86.5
Rb	1.7	2.2	1.5	1.6	0.9	1.5	2.1	3.4	0.5	0.8	0.1	1.5	1.0	0.2	1.1	1.6
Sr	132	274	159	164	200	182	181	114	87	84	106	138	124	123	161	86
Y	43.1	31.9	38.5	27.3	32.4	32.9	26.8	22.1	41.5	37.3	42.7	27.6	30.7	45.9	39.3	25.3
Zr	144.9	121.7	133.4	87.7	139.3	139.9	105.8	75.5	146.8	118.1	156.0	93.3	114.3	168.2	154.9	82.0
Nb	5.7	6.5	5.1	3.9	9.1	8.9	15.2	4.0	5.6	4.4	6.3	3.7	5.2	6.7	5.8	4.8
Ba	76	266	88	368	134	153	74	61	47	42	30	47	52	29	57	22
Hf	3.5	2.7	3.0	2.1	3.0	3.2	2.3	1.7	3.4	2.8	3.4	2.1	2.6	3.8	3.4	2.0
Ta	0.4	0.4	0.3	0.3	0.6	0.6	1.0	0.3	0.4	0.3	0.5	0.3	0.3	0.5	0.4	0.4
Th	0.3	0.5	0.3	0.2	0.8	0.9	1.0	0.4	0.3	0.3	0.5	0.3	0.3	0.5	0.5	0.5
La	5.6	6.2	5.9	3.9	7.5	7.6	8.4	3.8	6.1	5.2	7.1	4.5	4.7	7.0	6.6	4.9
Ce	16.5	16.0	16.5	11.3	18.2	18.8	20.0	10.5	17.7	15.0	20.1	12.5	13.5	20.2	18.4	12.7
Pr	2.8	2.3	2.6	1.8	2.5	2.6	2.6	1.6	2.8	2.4	3.0	1.9	2.1	3.1	2.8	1.9
Nd	15.2	11.7	13.5	9.3	12.3	12.9	12.2	7.9	14.6	12.5	15.5	9.8	10.9	16.4	14.1	9.4
Sm	4.9	3.5	4.3	3.0	3.6	3.8	3.2	2.4	4.6	4.0	4.7	3.0	3.4	5.1	4.3	2.9
Eu	1.3	1.2	2.2	1.0	1.3	1.3	1.1	0.9	1.5	1.4	1.4	0.9	1.2	1.6	1.5	1.1
Gd	5.7	4.2	5.2	3.7	4.3	4.6	3.7	3.0	5.7	4.9	5.7	3.6	4.2	6.2	5.3	3.5
Tb	1.1	0.7	0.9	0.6	0.8	0.8	0.6	0.5	1.0	0.9	1.0	0.6	0.7	1.1	0.9	0.6
Dy	6.9	5.0	6.0	4.4	5.1	5.4	4.3	3.6	6.7	5.9	6.8	4.3	5.0	7.4	6.2	4.1
Ho	1.4	1.0	1.2	0.9	1.0	1.1	0.8	0.7	1.3	1.2	1.4	0.9	1.0	1.5	1.2	0.8
Er	4.1	2.9	3.5	2.5	3.0	3.1	2.5	2.1	4.0	3.4	4.0	2.6	2.9	4.3	3.7	2.4
Tm	0.6	0.5	0.5	0.4	0.5	0.5	0.4	0.3	0.6	0.5	0.6	0.4	0.5	0.7	0.6	0.4
Yb	4.3	2.9	3.5	2.6	3.0	3.1	2.5	2.1	4.0	3.4	4.0	2.5	2.9	4.4	3.7	2.4
Lu	0.7	0.5	0.6	0.4	0.5	0.5	0.4	0.3	0.6	0.5	0.6	0.4	0.5	0.7	0.6	0.4

5. Discussion

5.1. Implications of the U–Pb results

The most immediate implication of the new $^{206}Pb/^{238}U$ age is that the SSVF is not an outlying fragment of the ~94–89 Ma Caribbean Oceanic Plateau (Kerr et al., 2003; Wadge and Macdonald, 1985) but represents magmatic activity during the Lower Cretaceous at ~135 Ma. Given its structural relationship with the Great Arc and the margin of Trinidad, and close temporal association with the passive margin sediments of the Toco Formation, we conclude that the SSVF was erupted in the proto-Caribbean seaway offshore from northern South America. The bulk of the SSVF does not contain large extractable zircons suitable for fission track analysis, so the ~108 Ma ages obtained by Algar et al. (1998) from the Toco Formation are unrelated to the SSVF. There is also an isotopic mismatch between the Toco Formation sandstone and the felsic, probably zircon-rich volcanic rocks found within the SSVF (Fig. 5). The unradiogenic Nd–Hf isotope signature of the Toco Formation sandstone is incompatible with its origin as detritus from the Caribbean Great Arc (cf. Nd–Hf isotope results in Neill et al., 2013). The simplest explanation for the ~108 Ma fission track ages from the Toco Formation is that they are the result of partial thermal resetting during metamorphism, whilst the Toco Formation itself was formed during the Barremian (~130–125 Ma) by accumulation of continent-derived sediments on the proto-Caribbean passive margin.

5.2. Tectonic setting of the mafic component of the SSVF

The lack of negative Nb–Ta, Ti, and Zr–Hf anomalies on the primitive mantle-normalised plots (Fig. 4b, d, f) and no enrichment of Th with respect to the MORB-OIB array on a Th/Yb vs. Ta/Yb diagram (Fig. 6a; Pearce, 1983) clearly indicates that these rocks are not subduction-related nor have they been influenced by typical continental crust. There is no clear temporal or geochemical correlation between the rocks of the SSVF and either the island arc-related suites of Tobago Island (Neill et al., 2013), or the Villa de Cura in Venezuela (Unger et al., 2005). Given that the SSVF presently lies to the south and east of the bulk of the Great Arc, its non-subduction-related geochemical signature further confirms an origin in the proto-Caribbean realm.

Incompatible trace element ratios in mafic rocks can be used to investigate the mantle source of the mafic SSVF as such ratios are largely unaffected by modest degrees of magmatic differentiation. The flat chondrite- and primitive mantle-normalised HREE patterns all indicate a shallow, spinel-facies source (<75 km). On Fig. 6a, the SSVF samples extend to high Ta/Yb ratios within the MORB-OIB array, normally interpreted to indicate low degrees of partial melting of depleted mantle or melting of an incompatible element-enriched source. The Nb/Y vs. Zr/Y plot (after Fitton et al., 1997; Fig. 6b), has previously been applied to the Caribbean region to distinguish rocks derived from incompatible trace element enriched or MORB-type mantle sources in the Caribbean

San Souc i—felsic rocks		Toco sandstone	El Copey meta-volcanic rocks			Siquisique gabbros					Siquisique basalts				
INSS7.1	INSS7.3	INSS5.1	AK01	AK02	AK05	AK19	AK21	AK22	AK27	AK28	AK20	AK23	AK24	AK25	AK26
65.21	64.45	81.28	47.59	48.99	47.82	52.23	49.71	49.15	49.12	48.43	49.89	48.23	50.53	49.01	48.82
0.56	0.51	0.62	1.64	1.63	1.87	0.99	1.11	1.24	1.07	0.97	1.43	2.21	1.78	1.42	1.71
14.73	16.98	8.80	15.77	16.05	15.48	15.96	16.68	16.40	13.93	16.00	14.49	13.51	14.10	15.24	14.04
5.61	4.37	2.35	11.53	9.89	11.29	9.64	9.55	9.88	7.07	9.22	10.15	15.01	13.05	10.46	12.54
0.08	0.10	bd	0.18	0.21	0.23	0.13	0.17	0.16	0.10	0.14	0.18	0.23	0.20	0.19	0.21
2.38	1.95	0.31	7.57	7.42	7.31	7.46	7.04	7.38	7.54	6.66	8.09	6.51	7.13	8.16	7.39
2.54	2.54	0.43	7.87	9.27	10.18	7.96	10.31	9.88	12.96	11.10	9.34	8.82	9.34	9.84	10.07
6.43	7.45	0.57	1.30	1.55	1.17	4.00	2.95	2.93	3.12	3.23	3.47	2.93	2.99	2.99	3.40
0.08	0.12	1.25	0.14	0.38	0.06	0.59	0.44	0.42	0.06	0.13	0.23	0.31	0.42	0.38	0.16
0.25	0.29	0.04	0.15	0.14	0.18	0.18	0.11	0.11	0.12	0.07	0.15	0.19	0.16	0.14	0.16
2.26	1.66	3.77	4.47	3.48	2.61	2.40	1.93	2.10	3.14	3.17	2.56	1.80	1.58	2.64	2.52
100.12	100.44	99.44	98.28	99.01	98.27	101.56	100.02	99.66	98.22	99.15	100.01	99.81	101.31	100.51	101.06
8.0	7.2	7.1	43.1	44.5	38.7	39.3	41.3	43.9	41.1	42.5	45.0	46.4	47.2	45.2	47.2
63.7	52.7	42.5	301.5	330.1	326.2	183.7	248.4	264.6	202.9	234.7	265.4	383.8	330.0	273.4	329.0
45.2	25.7	34.6	310.1	336.4	149.5	335.3	439.0	383.7	79.6	166.1	337.7	125.0	143.1	339.5	225.4
13.4	7.4	5.6	48.6	49.0	31.4	37.2	36.4	37.8	30.2	33.7	42.0	50.0	42.2	43.8	44.2
bd	bd	bd	128.0	153.9	105.0	93.9	84.6	71.6	53.2	62.9	89.3	81.9	63.2	95.2	67.1
0.9	1.2	55.1	3.8	13.9	0.6	9.5	7.5	7.0	0.5	1.6	3.5	5.1	7.4	5.3	2.1
123	271	70	25	29	225	260	275	310	154	166	236	187	239	232	154
26.5	26.7	29.9	36.3	39.2	42.8	40.0	27.2	27.5	32.5	22.8	30.3	47.8	40.6	30.6	38.2
340.4	476.3	659.9	117.8	110.6	144.9	159.0	76.9	73.0	108.3	64.1	103.3	141.3	115.4	102.8	117.1
52.6	92.2	14.7	6.0	6.2	10.0	5.7	2.5	2.8	3.2	1.9	5.3	4.9	3.8	5.1	4.5
23	66	161	73	235	124	313	257	278	69	97	155	205	278	139	97
6.3	8.5	14.5	2.7	2.6	3.5	3.8	1.9	1.9	2.7	1.7	2.5	3.5	3.0	2.5	3.0
3.6	6.2	1.1	0.4	0.4	0.6	0.4	0.1	0.2	0.2	0.1	0.3	0.3	0.2	0.3	0.3
6.4	10.6	12.4	0.4	0.5	0.7	0.6	0.2	0.2	0.3	0.2	0.3	0.3	0.3	0.3	0.3
38.0	54.5	31.8	5.3	6.3	8.4	7.4	3.7	3.3	3.5	2.8	4.6	6.1	5.5	5.2	5.2
69.1	95.9	70.2	14.5	14.3	20.1	19.4	9.9	8.6	10.0	7.6	12.0	16.8	14.2	13.3	14.5
6.8	9.1	7.7	2.4	2.3	3.1	2.8	1.6	1.5	1.5	1.2	2.0	2.6	2.3	2.2	2.3
23.5	29.2	28.7	11.5	11.6	15.5	13.8	8.3	7.9	8.2	6.1	10.0	13.5	12.0	10.7	11.8
4.1	4.7	5.3	3.6	3.6	4.5	4.1	2.7	2.7	2.9	2.1	3.2	4.5	3.9	3.3	3.8
1.2	1.3	0.8	1.3	1.3	1.6	1.2	1.0	1.0	1.2	0.9	1.1	1.6	1.4	1.1	1.3
4.1	4.4	4.5	4.7	5.0	5.7	5.2	3.6	3.6	4.1	2.9	4.1	6.1	5.3	4.3	5.1
0.6	0.7	0.7	0.8	0.9	1.0	0.9	0.6	0.6	0.8	0.5	0.7	1.1	0.9	0.8	0.9
4.0	4.0	4.5	5.5	6.2	6.7	6.1	4.3	4.4	5.1	3.6	4.8	7.2	6.4	5.0	6.2
0.8	0.8	0.9	1.1	1.3	1.4	1.3	0.9	0.9	1.0	0.8	1.0	1.5	1.3	1.0	1.3
2.5	2.5	2.8	3.5	3.8	4.1	3.9	2.7	2.7	3.1	2.2	2.9	4.6	3.9	2.9	3.7
0.4	0.4	0.5	0.5	0.5	0.6	0.6	0.4	0.4	0.5	0.4	0.5	0.7	0.6	0.5	0.6
2.6	2.8	3.3	3.2	3.5	3.8	3.8	2.5	2.5	3.0	2.1	2.7	4.4	3.8	2.8	3.5
0.4	0.5	0.6	0.5	0.6	0.6	0.6	0.4	0.4	0.5	0.3	0.4	0.7	0.6	0.4	0.6

region (e.g., Kerr et al., 2002; Neill et al., 2011). On Fig. 6b most mafic SSVF rocks plot just below the lower tramline, similar to N-MORB, whilst the remaining samples plot within the tramlines. Variable degrees of partial melting of a homogeneous source generate trends parallel to the tramlines (Fitton et al., 1997), so the SSVF is likely to be derived from the partial melting of a heterogeneous source with variable depletion or enrichment in incompatible trace elements. The most incompatible element-enriched mafic sample analysed for isotopes (INSS3c) is isotopically similar to the other mafic samples (Table 3), so there is no clear evidence for mixing between less radiogenic melts and the mafic volcanic rocks. Indeed the lack of any obvious relationship between isotope and trace element signatures in the mafic rocks means that any heterogeneities in the mantle source are likely to have been formed in the recent geological past.

These findings can be used to address the role of sub-continental lithosphere during rifting in the region. Mantle peridotites from the Tinaquillo lherzolite massif in Venezuela (Ostos et al., 2005; Fig. 1) have radiogenic isotope ratios (εHf up to + 50) which are decoupled from the terrestrial array to high εHf for a given εNd value (Choi et al., 2007; Fig. 4). This anomaly is taken to reflect an origin in the subduction-modified South American sub-continental lithosphere (Choi et al., 2007). Less extreme decoupling was reported in the Lower Cretaceous North Coast Schist of Tobago (Fig. 5), and interpreted as mixing between asthenospheric sources and rifted lithospheric fragments during growth of the southern portion of the inter-American Arc whilst it lay far to the west of its present location, in the eastern Pacific realm (Neill et al., 2012). The decoupled isotopic signatures of the South American sub-continental lithosphere are not present in the SSVF or other exposures in Venezuela, so it is assumed that these rocks formed from partial melts of convecting asthenosphere beneath the proto-Caribbean seaway away from the influence of sub-continental lithospheric mantle.

5.3. Modelling the extent of partial melting to form the San Souci Volcanic Group

We have calculated REE, Zr and Nb concentrations in melts using non-modal batch partial melt equations (Shaw, 2005) for depleted-, average and enriched-depleted MORB mantle sources (D-DMM, DMM and E-DMM, respectively) (Workman and Hart, 2005), and a hypothetical oceanic plateau source consisting of primitive mantle from which 1% average continental crust has been extracted (Fitton and Godard, 2004). Batch and fractional melting models are comparable at low degrees of partial melting (<10%, Shaw, 2005). There is little fractionation of the MREE/HREE in these mafic rocks ($Dy/Yb_{PMN} = 1.1$), ruling out melting of garnet peridotite, so a simple spinel lherzolite starting composition

was used, with proportions of mineral phases from Johnson et al. (1990) and partition coefficients from Pagé et al. (2009). Partial melting curves are plotted on Fig. 7a along with the SSVF mafic rocks. Since olivine is not present in the analysed rocks, and they are clearly not primary melts, we have also attempted to account for fractional crystallisation by subjecting some of the calculated partial melts to ~20% Rayleigh fractionation of an assemblage containing olivine and Cr-spinel in the ratio 9:1. The results have been normalised to Primitive Mantle and are presented on Fig. 7b for comparison with the low and high Zr/Nb samples from San Souci.

No single starting composition adequately models the spread of data from the SSVF—or indeed for data from outcrops at El Copey and Siquisique in Venezuela (Kerr et al., 2009). Partial melt curves (Fig. 7a) show that the composition of the majority of the SSVF rocks can be modelled by 2–7% melting of a range of sources from D-DMM to E-DMM. As indicated by the non-linear spread of samples on Fig. 7b and variable Zr/Nb ratios (7–27), the mantle source of the SSVF was heterogeneous, and this is borne out by partial melt modelling. Fig. 7b shows that the overall shape of the trace element patterns may be reasonably reproduced by partial melting of heterogeneous sources followed by removal of olivine and spinel. Further fractional crystallisation of clinopyroxene and plagioclase may be necessary to raise incompatible element concentrations to those observed in the analysed samples without significantly affecting elemental ratios.

5.4. Causes of melting

The degree of partial melting (<7%) indicated by the models are similar to the lowest reported figures for mid-ocean ridges (Hellebrand et al., 2001) but much lower than typical high-temperature plume-related settings (e.g., Hastie and Kerr, 2010). The fact that melting took place within the spinel stability field indicates that the SSVF was not formed by melting beneath thick oceanic lithosphere as is more typically the case for ocean island basalts. The lack of any geochemical or isotopic signatures typical of the melting of sub-continental lithosphere, or crustal contamination, indicates that by the time the SSVF formed in the Early Cretaceous, rifting was well advanced. Overall, the exact interpretation of how the SSVF formed depends upon whether or not the SSVF was erupted in the same location as the Toco Formation. If so, the SSVF must have formed on a passive margin, perhaps as a seamount (Algar, 1993), although the exact trigger for melting in this scenario is unclear. Alternatively, Pindell and Kennan (2001) argue that during the Late Jurassic–Early Cretaceous, a transform fault system developed between Yucatan (Mexico) and the northern coast of South America coupled to a spreading axis within the proto-Caribbean Seaway to the northeast of the South American margin (Fig. 8). This fault system would extend close enough to South America to receive clastic input from the continent, and could have been the site of extension-related magmatic activity.

5.5. Source of the felsic samples

As there are only two felsic samples, it is difficult to determine their origin and differentiation history. Low concentrations of Ni (~14 ppm), Cr (~35 ppm) and MgO (~2.1 wt.%) cannot be diagnostic of a mantle or crustal source given that the samples are highly evolved. However, their extreme LREE and HFSE enrichment and slightly less radiogenic isotope signatures compared to the mafic rocks indicates these are not simply highly fractionated lavas coeval with the mafic rocks. The felsic samples are enriched in HFSE except Ti, and have concave REE patterns with moderate HREE concentrations and $Dy/Yb_{CN} < 1$ (Fig. 4c–d). These patterns are dissimilar to many common rock types: in particular the REE patterns with no significant HREE depletion and the low Ti concentrations are unlike typical ocean island basalts.

The only samples we have found with similar trace element patterns to the SSVF felsic rocks are the felsic volcanic rocks of the Aigüa Series and the Valle Chico Igneous Complex, both from the Lower Cretaceous of Uruguay, formed at the southern edge of the Parana-Etendeka continental flood basalt province (Kirstein et al., 2000; Lustrino et al., 2005). These rocks have low Ti concentrations that have been proposed to be the result of extensive fractionation, but very high Zr and Nb which were attributed to complexing of these elements due to a high flux of volatiles from underlying mafic magmas (e.g., Hildreth, 1981; Kirstein et al., 2000). The Aigüa rocks, which have less radiogenic $^{143}Nd/^{144}Nd$ compared to the felsic SSVF samples, have been attributed to melting of pre-existing Uruguayan mafic lower crust during rifting and plume magmatism (Kirstein et al., 2000). It is possible that the San Souci felsic rocks were evolved melts of young isotopically distinct lower crust, perhaps proto-Caribbean oceanic material from the earliest phase of spreading, with volatiles derived from ongoing mafic magmatism helping induce complexing of HFSE.

Table 3
Age-corrected radiogenic isotope results for San Souci (135 Ma), El Copey (135 Ma) and Siquisique (90 Ma).

Unit and Sample	$^{176}Hf/^{177}Hf$			εHf_i	$^{143}Nd/^{144}Nd$			εNd_i
	Measured	±2σ	Initial		Measured	±2σ	Initial	
San Souci Volcanic Formation								
Mafic								
INSS3c	0.283139	0.000005	0.283084	+14.0	0.513088	0.000006	0.512932	+9.1
INSS6.5	0.283156	0.000007	0.283093	+14.3	0.513089	0.000005	0.512925	+9.0
INSS7.2	0.283140	0.000006	0.283070	+13.5	0.513065	0.000012	0.512901	+8.5
Felsic								
INSS7.3	0.282956	0.000006	0.282936	+8.8	0.512856	0.000002	0.512770	+6.0
INSS7.1	0.283013	0.000008	0.282989	+10.6	0.512878	0.000003	0.512784	+6.2
Toco Formation								
INSS5.1	0.282066	0.000004	0.282052	−22.5	0.511782	0.000002	0.511740	−14.1
El Copey meta-basalts								
AK01	0.283138	0.000007	0.283071	+13.5	0.513083	0.000026	0.512918	+8.8
AK02	0.283141	0.000005	0.283065	+13.3	0.513061	0.000002	0.512895	+8.4
Siquisique basalts (b) and gabbro (g)								
AK20b	0.283150	0.000006	0.283109	+13.9	0.513117	0.000006	0.513004	+9.4
AK25b	0.283148	0.000012	0.283107	+13.8	0.513106	0.000005	0.512996	+9.2
AK19g	0.283144	0.000007	0.283097	+13.5	0.513115	0.000006	0.512998	+9.3

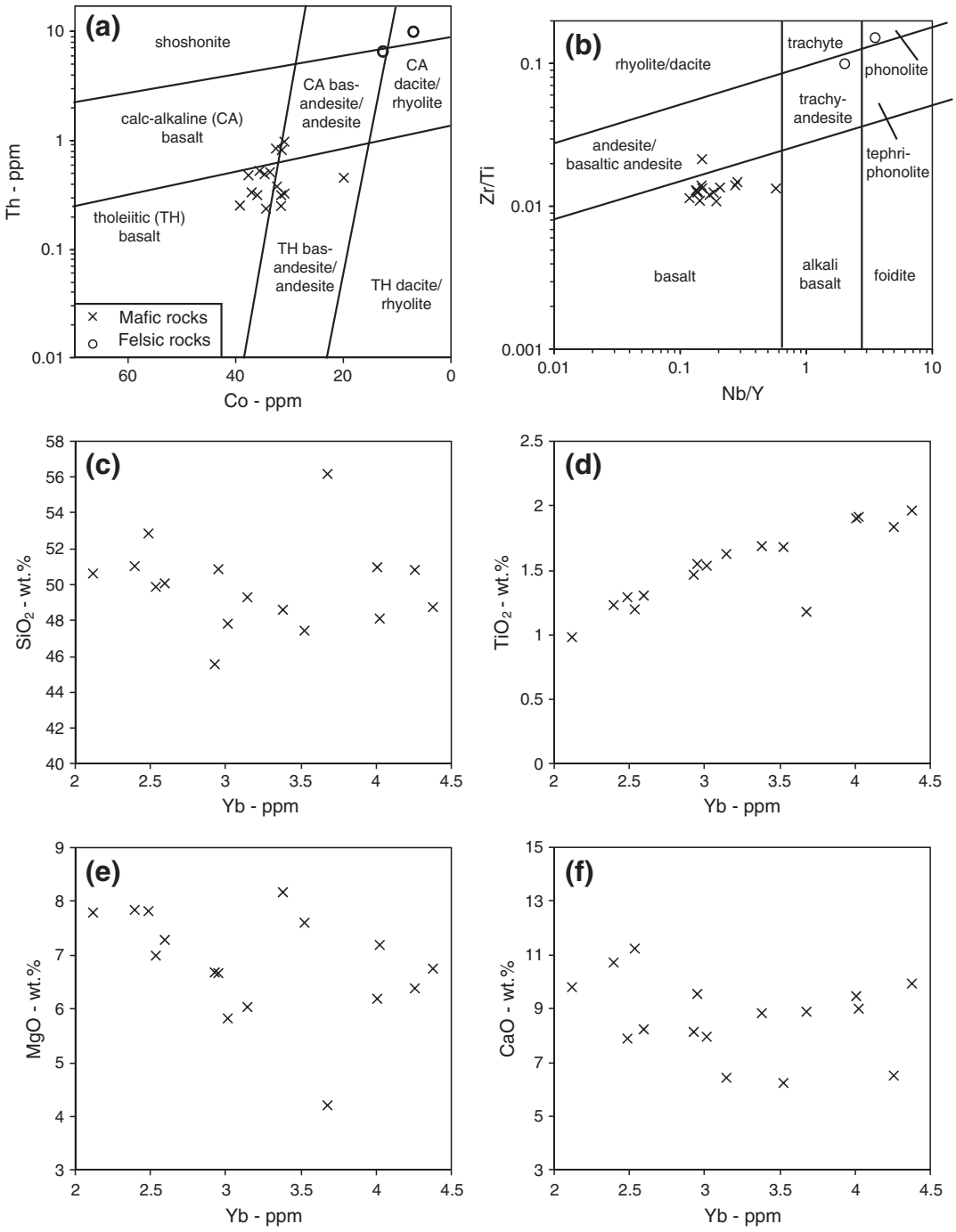

Fig. 3. Classification diagrams for the three locations followed by selected major element plots. (a) Th–Co classification from Hastie et al. (2007) and (b) Pearce, 1996. (c–f) SiO_2, TiO_2, MgO and CaO versus immobile incompatible element Yb.

A major difference between the Uruguayan rocks (Lustrino et al., 2005) and those from the SSVF is the concave REE patterns of the latter. Amphibole (also apatite and zircon) as a residual or fractionating phase may generate concave REE patterns as it is compatible with MREEs and moderately compatible with the HREEs (Davidson et al., 2013). Hydrous magmas that typically fractionate amphibole form in subduction-related environments, unlike the SSVF samples. Amphibole is therefore most likely to have been a residual phase in the source region. Positive Zr–Hf anomalies relative to the MREE may simply be a product of the fact that Zr and Hf are incompatible in amphibole (Klein et al., 1997) and high Zr/Hf ratios may have originated by low degrees of melting with residual pyroxene or other phases capable of fractionating the HFSE (David et al., 2000). Titanium and Nb–Ta usually display coupled behaviour as Nb and Ta are compatible in titanates (Nielsen and Beard, 2000; Tiepolo et al., 2001), but Nb and Ta are incompatible in high-Ti amphibole (e.g., Hilyard et al., 2000). Therefore residual high-Ti amphibole in a rutile-free lower crustal source region would produce the observed Nb–Ta–Ti anomalies of the felsic samples in a melt. Residual amphibole may thus represent an alternative to volatile complexing as a source of the unusual HFSE distributions in the SSVF.

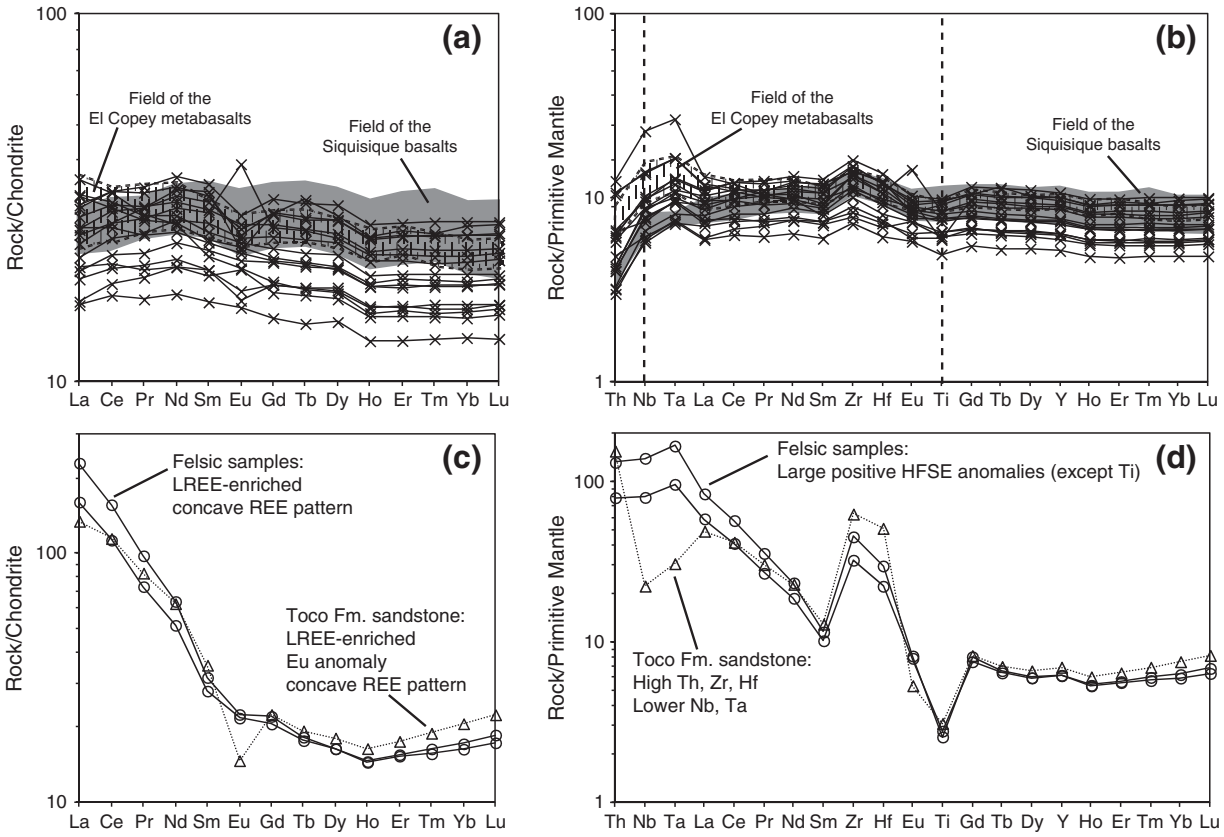

Fig. 4. Trace element plots from the SSVF with analyses of basalts from Venezuelan outcrops at El Copey (Barremian) and Siquisique (Turonian) for comparison (Kerr et al., 2009). See text for details. Chondrite normalisation from McDonough and Sun (1995); Primitive Mantle normalisation from Sun and McDonough (1989).

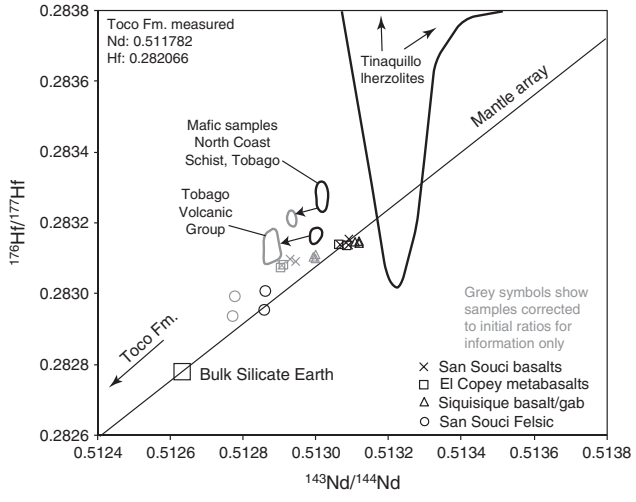

Fig. 5. Nd–Hf radiogenic isotope diagram comparing the SSVF with proto-Caribbean fragments at Siquisique and El Copey in Venezuela (Kerr et al., 2009), sub-continental lithosphere of the Tinaquillo lherzolite, Venezuela (Choi et al., 2007), the mafic Parlatuvier Formation of the North Coast Schist, Tobago, which has a sub-continental lithospheric component (Neill et al., 2012), and the Caribbean Great Arc rocks of the Tobago Volcanic Group (Neill et al., 2013). Bulk Silicate Earth and the mantle array are from Choi et al. (2007). The diagram shows measured ratios in black with grey symbols representing age-corrected ratios in order to demonstrate that there is little change in results and interpretation following correction.

6. Regional comparisons

6.1. Other basaltic outcrops in northern South America

Three other outcrops containing mafic volcanic rocks related to the proto-Caribbean realm are found in Venezuela. At El Copey on the Araya Peninsula (Fig. 1), meta-tuffs, pillow basalts and serpentinites are found in apparently conformable contact overlying the calcareous graphitic schists of the Neocomian–Barremian Carúpano Formation and themselves are overlain by the Güinimita Formation, a conglomeratic unit believed to be of Barremian–Aptian age (McMahon, 2000; Seijas, 1971). Assuming there are no faulted contacts, the El Copey metavolcanics are of Barremian age, and therefore penecontemporaneous with the SSVF and may indeed be an along-strike equivalent of the latter. Elemental and isotopic signatures are broadly comparable between the two units (Figs. 4–5; Kerr et al., 2009), and the ratio–ratio plots and partial melting models indicate ~5% partial melting of a slightly more enriched source than the bulk of the SSVF (Figs. 6–7).

The Siquisique basalts and gabbros of Los Algodones lie to the northwest of the Cordillera de la Costa (Fig. 1). Recent Ar–Ar dating (Kerr et al., 2009) and the ages of radiolarian-bearing cherts (Baumgartner et al., 2013) indicate a Late Cretaceous age of ~95–90 Ma for the Siquisique volcanic rocks. Earlier interpretations of the unit as a fragment of Jurassic proto-Caribbean crust (Bartok et al., 1985) were based on ammonites said to be collected from a Palaeogene mélange (Baumgartner et al., 2013). Geochemical comparisons and modelling show Siquisique was derived from modest degrees of melting (3–4%) of a heterogeneous mantle source roughly akin to depleted to average depleted MORB mantle (Fig. 7). Proto-Caribbean spreading had largely ceased by ~90 Ma (Müller et al., 1999; Seton et al., 2012), so it is likely that the Siquisique basalts and gabbros formed at a seamount or a localised extensional setting within the proto-Caribbean realm rather than at a true spreading ridge.

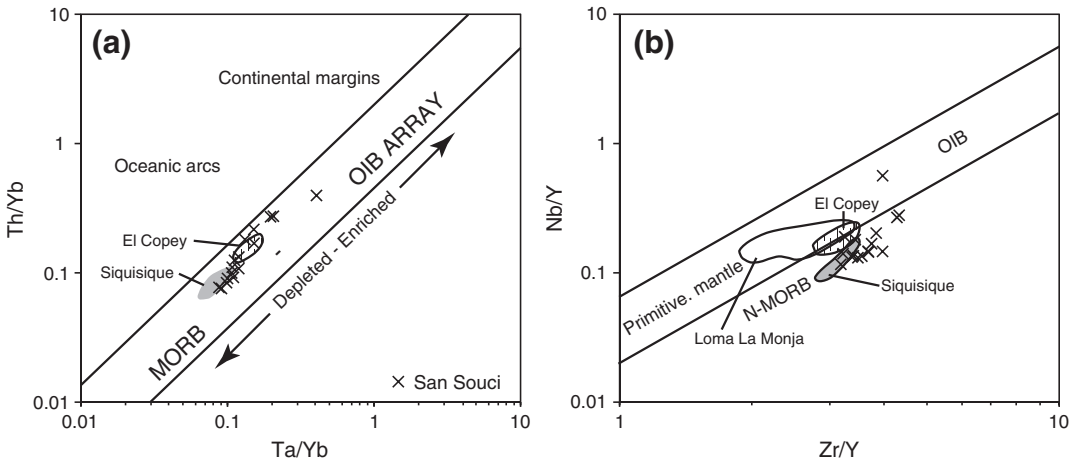

Fig. 6. Ratio–ratio plots. (a) Th/Yb vs Ta/Yb showing non-arc affinity of the studied samples (Pearce, 1983). (b) Nb/Y vs Zr/Y showing the range of incompatible element enriched and depleted rocks from the locations discussed in the text (Fitton et al., 1997).

Finally the Loma de Hierro belt immediately north of the Villa de Cura Klippe within the Cordillera de la Costa (Fig. 1) is another fragment of proto-Caribbean mafic crust (Urbani and Rodríguez, 2004). A new laser ablation $^{206}Pb/^{238}U$ zircon age of 127 + 1.9/−4.3 Ma has been obtained from a gabbroic sample (Marvin et al., 2013), comparable with the SSVF. There remains little geochemical information about the mafic rocks of Loma de Hierro: three whole rock major and trace element results showing incompatible element-depleted MORB-like signatures were obtained following fieldwork in 2004 (A.C. Kerr, unpublished data). The total outcrop of the Loma de Hierro covers at least 100 km^2 and should be a target for future detailed study.

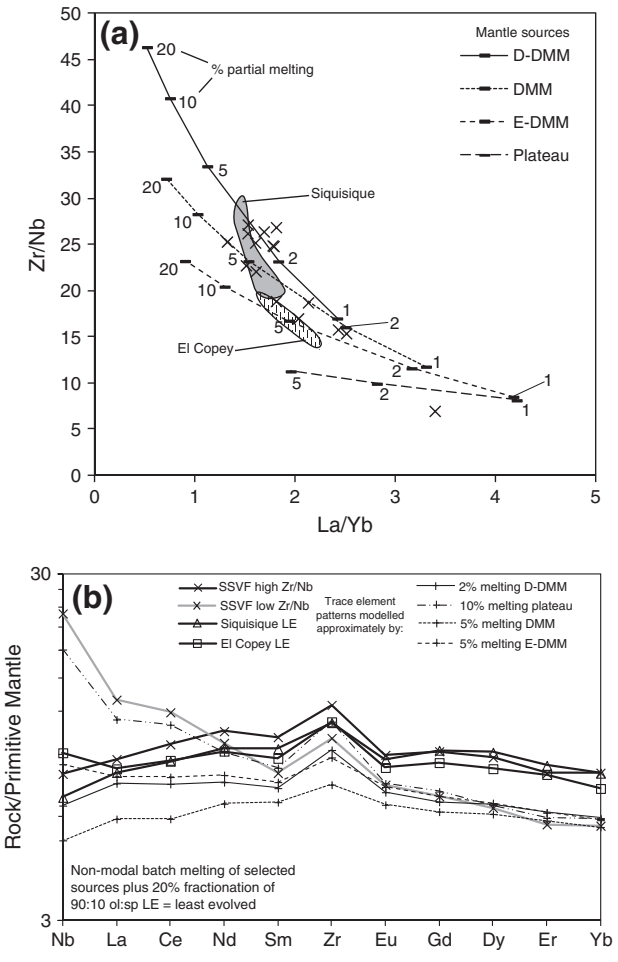

Fig. 7. Partial melting models. (a) Ratio–ratio plot with ticks indicating the degree of melting of different sources. (b) REE and HFSE plot for absolute concentrations of selected melts following fractional crystallisation of olivine and spinel. See text for full details.

6.2. Proto-Caribbean crust in the Greater or Lesser Antilles

There are further examples of proto-Caribbean material preserved within the present-day Greater or Lesser Antilles which may provide insights into the development of the seaway. Cretaceous inception of SW-dippingproto-Caribbean subduction resulted in the trapping of proto-Caribbean crustal and lithospheric mantle sections within the new 'Great Arc', some of which are discussed here. The Loma La Monja gabbros and basalts of the Cordillera Central, Hispaniola (Escuder Viruete et al., 2009), fall within the Iceland tramlines at slightly lower Zr/Y ratios than San Souci (Fig. 6b). The Loma La Monja complex is late Middle Jurassic in age, on the basis of radiolarian ages from overlying cherts of the El Aguacate Formation (Montgomery et al., 1994). These rocks are argued to be the product of low-degree melting in the garnet stability field followed by 15–20% melting of N-MORB- and E-MORB-like sources (Escuder Viruete et al., 2009). Escuder Viruete et al. (2009) proposed the presence of a mantle plume to explain the E-MORB source and high degree of partial melting. These figures for partial melting are indeed higher than those for typical spreading ridges (~10%) but slightly lower than the fast-spreading East Pacific Rise (Niu and Hékinian, 1997), so there is no clear evidence for a mantle plume origin for Loma La Monja aside from the incompatible element-enriched mantle source. Melting might also be focussed at a proto-Caribbean triple junction towards the western end of the Seaway related to opening of Mexican and Colombian back-arc basins (e.g., Pindell, 1993; Pindell and Kennan, 2001; Fig. 8).

In contrast, the Late Jurassic volcano-plutonic complexes of La Désirade, Guadeloupe, have a back-arc basin geochemical signature and are derived from depleted mantle (Neill et al., 2010). These rocks were probably formed in the westernmost proto-Caribbean close to the then east-dippinginter-American arc system (Fig. 8). Like Loma La Monja, La Désirade was accreted to the Great Arc during inception of SW-dipping subduction (Corsini et al., 2011; Neill et al., 2010). Apart from Tinaquillo in Venezuela, which may represent an intra-continental rift adjacent to the proto-Caribbean Seaway (Ostos et al., 2005), one of the few fragments of proto-Caribbean lithospheric mantle is found at Monte de Estado in south-west Puerto Rico (Jolly et al., 2008; Marchesi et al., 2011). Analysis of spinel and clinopyroxene compositions in the Monte del Estado peridotite indicates removal of 2–15% partial melt in the spinel stability field (Marchesi et al., 2011). This range

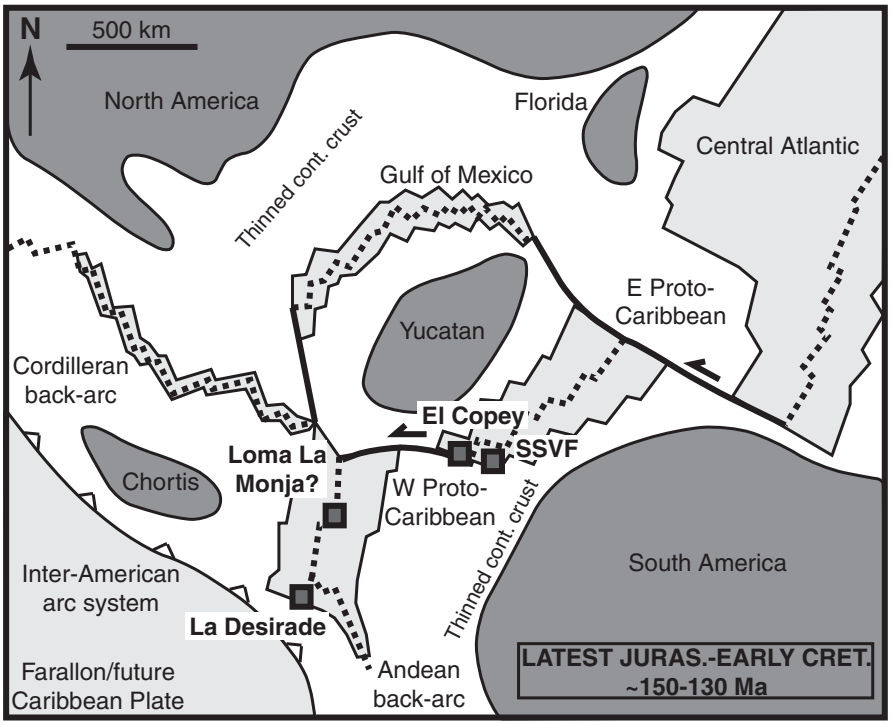

Fig. 8. Late Jurassic–Early Cretaceous palaeogeography after Pindell and Kennan (2001), showing probable location of proto-Caribbean fragments discussed in the text. La Désirade after Neill et al. (2010). Position of Loma La Monja (Hispaniola) (Escuder Viruete et al., 2009) is uncertain but likely to be in the western proto-Caribbean some distance from the inter-American subduction system. Dark grey: continental masses, white: thinned continental crust, light grey: oceanic crust.

extends slightly higher than for our analysed samples, and appears consistent with melting beneath a reasonably fast-spreading ridge; the exact palaeo-location within the proto-Caribbean realm is uncertain.

6.3. The break-up of Pangaea and importance to Caribbean tectonics

We have little evidence regarding a plume model for the *initiation* of proto-Caribbean rifting, or of any relationship between the studied proto-Caribbean rocks and the widespread 200 Ma Central Atlantic Magmatic Province (CAMP). Unfortunately, there has not been a Hf isotope study of CAMP magmatism with which to compare our results on altered rocks to seek common mantle sources. However, we note that the geochemical heterogeneities present in the SSVF and other locations are restricted to trace elements and not isotope signatures, so modification of their mantle sources had to have taken place recently before their formation. Heterogeneous proto-Caribbean mantle sources and locally enhanced degrees of partial melting might be explained by the contamination or fertilisation of the upper asthenosphere and lithosphere by the CAMP plume a few tens of Ma prior to the opening of the proto-Caribbean. Impingement of a plume beneath Pangaea may also have weakened the lithosphere and pre-disposed the region to rifting at a later date.

The Mesozoic tectonic evolution of the Caribbean region involves the onset of southwest-dipping subduction of proto-Caribbean crust beneath the 'Great Arc' starting at a contentious point in the Early or Late Cretaceous (e.g., Hastie et al., 2013; Pindell et al., 2011). This paper does not discuss this aspect of Caribbean tectonics, but it is pertinent to note the absence of large tracts of proto-Caribbean crust derived from high degrees of partial melting. This finding indicates that the proto-Caribbean crust was probably of normal (6–7 km) thickness, and would subduct beneath the inter-American Arc given the right tectonic circumstances. Those supporting Late Cretaceous initiation of subduction beneath the Great Arc argue for collision between the Caribbean Oceanic Plateau and the inter-American Arc (e.g., Burke, 1988; Kerr et al., 2003), but there is also significant support for an Early Cretaceous onset of SW-dipping subduction triggered by the fragmentation and stretching of the inter-American Arc and its conversion into a transpressive boundary during the westward drift of North America (e.g., Pindell et al., 2011). Others have argued for Early Cretaceous choking of the proto-Greater Antilles Arc trench by old (i.e. pre-95 Ma) plume-thickened Pacific crust, forcing a pre-Caribbean Oceanic Plateau subduction polarity reversal (Corsini et al., 2011; Lardeaux et al., 2013; Mauffrey and Leroy, 1997). The question of how young, thick and buoyant the proto-Caribbean crust was becomes important: any subduction polarity reversal or initiation would be aided by the presence of comparatively thin crust on the proto-Caribbean side of the inter-American Arc system (e.g., Stern, 2004).

7. Conclusions and recommendations

1) The San Souci Volcanic Formation is an Early Cretaceous unit in Trinidad containing mafic volcanic and hypabyssal rocks which originated close to the South American passive margin of the proto-Caribbean Seaway as the Americas drifted apart during the break-up of Pangaea.
2) Both the SSVF and the likely penecontemporaneous El Copey metavolcanic rocks and younger Siquisique basalts and gabbros (both in Venezuela) formed by <7% partial melting of a spinel lherzolite source containing both depleted and enriched components. Fragments of proto-Caribbean crust and lithospheric mantle found today in the Caribbean region confirm the presence of heterogeneous mantle sources across the proto-Caribbean at various times during rifting, but fail to demonstrate that there was a singular large-scale plume-related event during the Jurassic–Cretaceous in this region.
3) This work shows the potential for micro-zircon to be used as a revealing and reasonably precise chronometer in mafic rocks from the Caribbean region where other methods, such as Ar–Ar dating, fail. Further SIMS dating work to resolve the age of proto-

Caribbean crust and help resolve the age and origin of the CCOP could be fruitful.

4) Outcrops such as El Copey and Siquisique, and in particular the relatively unknown Loma de Hierro belt of the Cordillera de la Costa, require more detailed studies of their geochemical signatures, in a similar manner to this work, to help build a picture of the nature of proto-Caribbean spreading and development of the passive margin. Furthermore, there remains a need to understand clearly the origin and tectonic evolution of the Netherlands-Venezuelan Antilles, Aves Ridge, Villa de Cura, and Tobago Island subduction-related rocks in order to definitively reconstruct southern Caribbean tectonic history, and by proxy that of the Caribbean Plate as a whole.

Supplementary data to this article can be found online at http://dx.doi.org/10.1016/j.tecto.2014.04.019.

Acknowledgements

I.N. was supported by a Natural Environment Research Council (NERC) PhD studentship [NX/F00229X/1] whilst at Cardiff University. A NERC facilities committee grant-in-kind to A.C.K. and I.N. [IP/1064/1108] enabled radiogenic isotope work and a NERC small grant [NER/B/S/2001/00827] to A.C.K. allowed collection and analysis of Venezuelan samples. The ion microprobe facility at UCLA is partly supported by grant numbers 1029193 and 1339051 from the Instrumentation and Facilities Program, Division of Earth Sciences, National Science Foundation. Laura Cotton and Greta Robertson assisted with fieldwork in Trinidad. Iain McDonald and Ley Woolley are thanked for running the major and trace element analyses. We are grateful to Peter Bartok for discussions on Siquisique. Thanks to Hubert Whitechurch, an anonymous reviewer and editor Laurent Jolivet for their constructive comments on the manuscript.

References

Algar, S.T., 1993. Structural, stratigraphic, and thermo-chronological evolution of Trinidad. Unpublished PhD Thesis, Dartmouth College, Hanover, New Hampshire, 433 pages.

Algar, S.T., 1998. Tectonostratigraphic development of the Trinidad region. In: Pindell, J.L., Drake, C.L. (Eds.), Palaeogeographic Evolution and Non-glacial Eustacy, Northern South America. SEPM Special Publication, 58, pp. 87–109.

Algar, S.T., Pindell, J.L., 1991. Structural development of the Northern Ranges of Trinidad and implications for the tectonic development of the southeastern Caribbean. In: Gillezeau, K.A. (Ed.), Transactions of the Second Geological Conference of the Geological Society of Trinidad and Tobago. Petrotrin, Pointe-a-Pierre, Trinidad (281 pp.).

Algar, S.T., Pindell, J.L., 1993. Structure and deformation history of the Northern Ranges of Trinidad and adjacent areas. Tectonics 12, 814–829.

Algar, S.T., Heady, E.C., Pindell, J.L., 1998. Fission track dating in Trinidad: implications for provenance, depositional timing and tectonic uplift. In: Pindell, J.L., Drake, C.L. (Eds.), Palaeogeographic Evolution and Non-glacial Eustacy, Northern South America. SEPM Special Publication, 58, pp. 111–128.

Barr, K.W., 1962. The geology of the Toco District, Trinidad, West Indies, Pt. 1. Overseas Geology and Mineral Resources, 8, pp. 379–415.

Barr, K.W., 1963. The geology of the Toco District, Trinidad, West Indies, Pt. 2. Overseas Geology and Mineral Resources, 9, pp. 1–29.

Bartok, P., 1993. Prebreakup geology of the Gulf of Mexico-Caribbean: its relation to Triassic and Jurassic rift systems of the region. Tectonics 12, 441–459.

Bartok, P., Renz, O., Westermann, G.E.G., 1985. The Siquisique ophiolites, northern Lara State, Venezuela: a discussion on their middle Jurassic ammonites and tectonic implications. GSA Bull. 96, 1050–1055.

Baumgartner, P.O., Rojas-Agramonte, Y., Sandoval-Gutierrez, M., Urbani, F., García-Delgado, D., Garban, G., Pérez-Rodríguez, M., 2013. Late Jurassic break-up of the proto-Caribbean and circum-global circulation across Pangea. Geophysical Research Abstracts 15, 13408–13413.

Bezada, M.J., Magnani, M.B., Zelt, C.A., Schmitz, M., Levander, A., 2010. The Caribbean–South American Plate boundary at 65°W: results from wide-angle seismic data. J. Geophys. Res. Solid Earth 115, B8. http://dx.doi.org/10.1029/2009JB007070.

Blichert-Toft, J., 2001. On the Lu–Hf isotope geochemistry of silicate rocks. Geostand. Newslett. 25, 41–56.

Burke, K., 1988. Tectonic evolution of the Caribbean. Annu. Rev. Earth Planet. Sci. 16, 201–230.

Callegaro, S., Marzoli, A., Bertrand, H., Chiaradia, M., Reisberg, L., Meyzen, C., Bellieni, G., Weems, R.E., Merle, R., 2013. Upper and lower crust recycling in the source of CAMP basaltic dykes from southeastern North America. Earth Planet. Sci. Lett. 376, 186–199.

Cann, J.R., 1970. Rb, Sr, Zr and Nb in some ocean floor basaltic rocks. Earth Planet. Sci. Lett. 10, 7–11.

Chamberlain, K.R., Schmitt, A.K., Swapp, S.M., Mark Harrison, T., Swoboda-Colberg, N., Bleeker, W., Peterson, T.D., Jefferson, C.W., Khudoley, A.K., 2010. In situ U–Pb SIMS (IN-SIMS) micro-baddeleyite dating of mafic rocks: method with examples. Precambrian Res. 183, 379–387.

Choi, S.H., Mukasa, S.B., Andronikov, A.V., Marcano, M.C., 2007. Extreme Sr–Nd–Pb–Hf isotopic compositions exhibited by the Tinaquillo peridotite massif, Northern Venezuela: implications for geodynamic setting. Contrib. Mineral. Petrol. 153, 443–463.

Corsini, M., Lardeaux, J.M., Verati, C., Voitus, E., Balagne, M., 2011. Discovery of Lower Cretaceous synmetamorphic thrust tectonics in French Lesser Antilles (La Désirade Island, Guadeloupe): implications for Caribbean geodynamics. Tectonics 30, TC4005. http://dx.doi.org/10.1029/2011TC002875.

David, K., Schiano, P., Allégre, C.J., 2000. Assessment of the Zr/Hf fractionation in oceanic basalts and continental materials during petrogenetic processes. Earth and Planetary Science Letters 178, 285–301.

Davidson, J., Turner, S., Plank, T., 2013. Dy/Dy*: variations arising from mantle sources and petrogenetic processes. J. Petrol. 54, 525–537.

Escalona, A., Mann, P., 2010. Tectonics, basin subsidence mechanisms, and paleogeography of the Caribbean–South American plate boundary zone. Mar. Pet. Geol. 28, 8–39.

Escuder Viruete, J., Pérez-Estaún, A., Weis, D., 2009. Geochemical constraints on the origin of the late Jurassic proto-Caribbean oceanic crust in Hispaniola. Int. J. Earth Sci. 98, 407–425.

Escuder Viruete, J., Castillo-Carillón, M., Pérez-Estaún, A., 2014. Magmatic relationships between depleted mantle harzburgites, boninitic cumulate gabbros and subduction-related tholeiitic basalts in the Puerto Plata ophiolitic complex, Dominican Republic: Implications for the birth of the Caribbean island-arc. Lithos 196, 261–280.

Fitton, J.G., Godard, M., 2004. Origin and evolution of magmas on the Ontong Java Plateau. In: Fitton, J.G., Mahoney, J.J., Wallace, P.J., Saunders, A.D. (Eds.), Origin and Evolution of the Ontong Java Plateau. Geological Society of London Special Publication, 229, pp. 151–178.

Fitton, J.G., Saunders, A.D., Norry, M.J., Hardarson, B.S., Taylor, R.N., 1997. Thermal and chemical structure of the Iceland plume. Earth Planet. Sci. Lett. 153, 197–208.

Giunta, G., Beccaluva, L., Coltorti, M., Siena, F., Vaccaro, C., 2002. The southern margin of the Caribbean Plate in Venezuela: tectono-magmatic setting of the ophiolite units and kinematic evolution. Lithos 63, 19–40.

Hackley, P.C., Urbani, F., Karlsen, A.W., Garrity, C.P., 2005. Geologic shaded relief map of Venezuela. United States Geological Survey Open-File Report 2005-1038, 1:750 000, 2 sheets.

Hastie, A.R., Kerr, A.C., 2010. Mantle plume or slab window?: Physical and geochemical constraints on the origin of the Caribbean oceanic plateau. Earth-Science Reviews 98, 283–293.

Hastie, A.R., Kerr, A.C., Pearce, J.A., Mitchell, S.F., 2007. Classification of altered island arc rocks using immobile trace elements: development of the Th–Co discrimination diagram. J. Petrol. 48, 2341–2357.

Hastie, A.R., Mitchell, S.F., Treloar, P.J., Kerr, A.C., Neill, I., Barfod, D., 2013. Geochemical components in a Cretaceous island arc: the Th/La-$(Ce/Ce^*)_{Nd}$ diagram and implications for subduction initiation in the inter-American region. Lithos 162, 57–69.

Haxby, W.F., Melkonian, A.K., Coplan, J., Chan, S.-M., Ryan, W.B.F., 2010. GeoMapApp freeware software, v. 3.3.9. Lamont-Doherty Earth Observatory, Palisades, NY.

Heaman, L.M., LeCheminant, A.N., 1993. Paragenesis and U–Pb systematics of baddeleyite (ZrO_2). Chem. Geol. 110, 95–126.

Hellebrand, E., Snow, J.E., Dick, H.J.B., Hofmann, A.W., 2001. Coupled major and trace elements as indicators of the extent of melting in mid-ocean-ridge peridotites. Nature 410, 677–681.

Hildreth, W., 1981. Gradients in silicic magma chambers: implications for lithospheric magmatism. J. Geophys. Res. 86, 10153–10192.

Hill, R.I., 1993. Mantle plumes and continental tectonics. Lithos 30, 193–206.

Hilyard, M., Nielsen, R.L., Beard, J.S., Patino-Douce, A., Blencoe, J., 2000. Experimental determination of the partitioning behaviour of rare earth and high field strength elements between pargasitic amphibole and natural silicate melts. Geochim. Cosmochim. Acta 64, 1103–1120.

Hung, E.J., 2005. Thrust belt interpretation of the Serranía del Interior and Maturín subbasin, eastern Venezuela. In: Avé Lallemant, H.G., Sisson, V.B. (Eds.), Caribbean–South American Plate Interactions, Venezuela. GSA Special Paper, 394, pp. 251–270.

Jackson, T.A., Smith, T.E., Duke, M.J.M., 1991. The geochemistry of a metavolcanic horizon in the Maracas Formation, Northern Range, Trinidad: evidence of ocean floor basalt activity. In: Gillezeau, K.A. (Ed.), Transactions of the 2nd Geological Conference of the Geological Society of Trinidad and Tobago, Port of Spain, Trinidad, April 3–8, 1990, pp. 42–47.

Johnson, K.T.M., Dick, H.J.B., Shimizu, N., 1990. Melting in the oceanic upper mantle: an ion microprobe study of diopsides in abyssal peridotites. J. Geophys. Res. 95, 2661–2678.

Jolly, W.T., Lidiak, E.G., Dickin, A.P., 2008. Bimodal volcanism in northeast Puerto Rico and the Virgin Islands (Greater Antilles island arc): genetic links with Cretaceous subduction of the mid-Atlantic ridge Caribbean spur. Lithos 103, 393–414.

Kerr, A.C., Tarney, J., Marriner, G.F., Klaver, G.Th., Saunders, A.D., Thirlwall, M.F., 1996. The geochemistry and petrogenesis of the late-Cretaceous picrites and basalts of Curaçao, Netherlands Antilles: a remnant of an oceanic plateau. Contrib. Mineral. Petrol. 124, 29–43.

Kerr, A.C., Tarney, J., Kempton, P.D., Spadea, P., Nivia, A., Marriner, G.F., Duncan, R.A., 2002. Pervasive mantle plume head heterogeneity: evidence from the late Cretaceous Caribbean–Colombian oceanic plateau. J. Geophys. Res. 107, B7. http://dx.doi.org/10.1019/2001JB000790.

Kerr, A.C., White, R.V., Thompson, P.M.E., Tarney, J., Saunders, A.D., 2003. No oceanic plateau—no Caribbean Plate? The seminal role of an oceanic plateau in Caribbean Plate evolution. In: Bartolini, C., Buffler, R.T., Blickwede, J.F. (Eds.), The circum-Gulf of Mexico and the Caribbean: hydrocarbon habitats, basin formation and plate

tectonics, 79. American Association of Petroleum Geologists Memoir, Tulsa, pp. 126–168.
Kerr, A.C., Neill, I., Urbani, F., Spikings, R., Barry, T., Tarney, J., 2009. The Siquisique basalts and gabbros, Los Algodones, Venezuela: Late Cretaceous oceanic plateau formed within the proto-Caribbean Plate. AGU Fall Meeting Abstracts (V41C-2193).
Kirstein, L.A., Peate, D.W., Hawkesworth, C.J., Turner, S.P., Harris, C., Mantovani, M.S.M., 2000. Early Cretaceous basaltic and rhyolitic magmatism in southern Uruguay associated with the opening of the South Atlantic. J. Petrol. 41, 1413–1438.
Klein, M., Stosch, H.-G., Shimizu, N., 1997. Experimental partitioning of high field strength and rare earth elements between clinopyroxene and garnet in andesitic to tonalitic systems. Geochim. Cosmochim. Acta 64, 99–115.
Krogh, T.E., Corfu, F., Davis, D.W., Dunning, G.R., Heaman, L.M., Kamo, S.L., Machado, N., Greenough, J.D., Nakamura, E., 1987. Precise U–Pb isotopic ages of diabase dykes and mafic to ultramafic rocks using trace amounts of baddeleyite and zircon. In: Halls, H.C., Fahrig Mafic, W.F. (Eds.), Dyke swarms. Geological Association of Canada Special Paper, 34, pp. 147–152.
Lardeaux, J.-M., Münch, P., Corsini, M., Corneé, J.-J., Verati, C., Lebrun, J.-F., Quillévéré, F., Melinte-Dobrinescu, M., Léticée, J.-L., Fietzke, J., Mazabraud, Y., Cordey, F., Randrianasolo, A., 2013. La Désirade Island (Guadeloupe, French West Indies): a key target for deciphering the role of reactivated tectonic structures in Lesser Antilles arc building. Bull. Geol. Soc. Fr. 184, 21–34.
Loewen, M.W., Duncan, R.A., Kent, A.J.R., Krawl, K., 2013. Prolonged plume volcanism in the Caribbean Large Igneous Province: new insights from Curaçao and Haiti. Geochem. Geophys. Geosyst. 14 (10), 4241–4259.
Lustrino, M., Melluso, L., Brotzu, P., Gomes, C.B., Morbidelli, L., Muzio, R., Ruberti, E., Tassinari, C.C.G., 2005. Petrogenesis of the Early Cretaceous Valle Chico igneous complex (SE Uruguay): relationships with Paraná–Etendeka magmatism. Lithos 82, 407–434.
Marchesi, C., Jolly, W.T., Lewis, J.F., Garrido, C.J., Proenza, J.A., Lidiak, E.G., 2011. Petrogenesis of fertile mantle peridotites from the Monte del Estado massif (Southwest Puerto Rico): a preserved section of Proto-Caribbean lithospheric mantle? Geol. Acta 9, 289–306.
Maresch, W.V., 1974. Plate tectonics origin of the Caribbean Mountain System of northern South America: discussion and proposal. Geol. Soc. Am. Bull. 85, 669–682.
Maresch, W.V., Kluge, R., Baumann, A., Pindell, J.L., Krückhans-Lueder, G., Stanek, K.P., 2009. The occurrence and timing of high-pressure metamorphism on Margarita Island, Venezuela: a constraint on Caribbean–South America interaction. In: James, K.H., Lorente, M.A., Pindell, J.L. (Eds.), The Origin and Evolution of the Caribbean Plate. Geological Society of London Special Publications, 328, pp. 705–741.
Marvin, B., Valencia, V., Grande, S., Urbani, F., Hurtado, R., 2013. Geocronología U–Pb en cristales de zircón de la metadiorita de la Guacamaya, gabro de la ofiolita de Loma de Hierro y gabro de El Chacao, estados Aragua y Guárico. V Simposio Venezolano de Geociencias de las Rocas Ígneas y Metamórficas, Caracas, Venezuela, 28th–29th November, 2013.
Mauffrey, A., Leroy, S., 1997. Seismic stratigraphy and structure of the Caribbean igneous province. Tectonophysics 283, 61–104.
McDonald, I., Viljoen, K.S., 2006. Platinum-group element geochemistry of mantle eclogites: a reconnaissance study of xenoliths from the Orapa kimberlite, Botswana. Appl. Earth Sci. Trans. Inst. Min. Metall. B 115, 81–93.
McDonough, W.F., Sun, S.-S., 1995. The composition of the Earth. Chem. Geol. 120, 223–253.
McHone, J.G., 2000. Non-plume magmatism and rifting during the opening of the central Atlantic Ocean. Tectonophysics 316, 287–296.
McMahon, C.E., 2000. Evaluating the effects of oblique collision between the Caribbean and South American plates using geochemistry from igneous and metamorphic bodies in Northern Venezuela. Unpublished PhD thesis, University of Notre Dame, 227 pages.
Montgomery, H., Pessagno Jr., E.A., Pindell, J.L., 1994. A 195 Ma terrane in a 165 Ma ocean: Pacific origin of the Caribbean Plate. GSA Today 4, 1–6.
Muessig, K.W., 1984. Structure and Cenozoic tectonics of the Falcon Basin, Venezuela, and adjacent areas. GSA Mem. 162, 217–230.
Müller, R.D., Royer, J.-Y., Cande, S.C., Roest, W.R., Maschenkov, S., 1999. New constraints on the Late Cretaceous/Tertiary plate tectonic evolution of the Caribbean. In: Mann, P. (Ed.), Caribbean Basins. Sedimentary Basins of the World, 4. Elsevier, Amsterdam, pp. 33–59.
Münker, C., Weyer, S., Scherer, E., Mezger, K., 2001. Separation of high field strength elements (Nb, Ta, Zr, Hf) and Lu from rock samples for MC-ICPMS measurements. Geochem. Geophys. Geosyst. 2 (2001GC000183).
Neill, I., Gibbs, J.A., Hastie, A.R., Kerr, A.C., 2010. Origin of the volcanic complexes of La Désirade, Lesser Antilles: implications for tectonic reconstruction of the Late Jurassic to Cretaceous Pacific-proto-Caribbean margin. Lithos 120, 407–420.
Neill, I., Kerr, A.C., Hastie, A.R., Stanek, K.P., Millar, I.L., 2011. Origin of the Aves Ridge and Dutch-Venezuelan Antilles: interaction of the Cretaceous 'Great Arc' and Caribbean–Colombian Oceanic Plateau. J. Geol. Soc. Lond. 168, 333–348.
Neill, I., Kerr, A.C., Hastie, A.R., Pindell, J.L., Millar, I.L., Atkinson, N., 2012. Age and petrogenesis of the Lower Cretaceous North Coast Schist of Tobago, a fragment of the proto-Greater Antilles inter-American arc system. J. Geol. 120, 367–384.
Neill, I., Kerr, A.C., Hastie, A.R., Pindell, J.L., Millar, I.L., 2013. The Albian–Turonian island arc rocks of Tobago, West Indies: geochemistry, petrogenesis, and Caribbean Plate tectonics. J. Petrol. 54, 1607–1639.
Nielsen, R.L., Beard, J.S., 2000. Magnetite-meltHFSE partitioning. Chem. Geol. 164, 21–34.
Niu, Y., Hékinian, R., 1997. Spreading rate-dependence of the extent of mantle melting beneath mid-ocean ridges. Nature 385, 326–329.
Nowell, G.M., Parrish, R.R., 2001. Simultaneous acquisition of isotope compositions and parent/daughter ratios by non-isotope dilution solution-mode plasma ionisation multi-collector mass spectrometry (PlMMS). In: Holland, G., Tanner, S.D. (Eds.), Plasma Source Mass Spectrometry—The New Millenium. Royal Society of Chemistry, Cambridge, pp. 298–310.
Ostos, M., Sisson, V.B., 2005. Geochemistry and tectonic setting of igneous and metaigneous rocks of northern Venezuela. In: Avé Lallemant, H.G., Sisson, V.B. (Eds.), Caribbean–South American Plate Interactions, Venezuela. GSA Special Paper, 394, pp. 119–156.
Ostos, M., Avé Lallemant, H.G., Sisson, V.B., 2005. The Alpine-type Tinaquillo peridotite complex, Venezuela: fragment of a Jurassic rift zone? In: Avé Lallemant, H.G., Sisson, V.B. (Eds.), Caribbean–South American Plate Interactions, Venezuela. GSA Special Paper, 394, pp. 207–222.
Pagé, P., Bédard, J.H., Tremblay, A., 2009. Geochemical variations in a depleted fore-arc mantle: the Ordovician Thetford Mines Ophiolite. Lithos 113, 21–47.
Pearce, J.A., 1983. Role of the sub-continental lithosphere in magma genesis at active continental margins. In: Hawkesworth, C.J., Norrry, M.J. (Eds.), Continental Basalts and Mantle Xenoliths. Shiva, Nantwich, pp. 230–249.
Pearce, J.A., 1996. A users guide to basalt discrimination diagrams. In: Wyman, D.A. (Ed.), Trace element geochemistry of volcanic rocks: Applications for massive sulphide exploration. Geological Association of Canada Short Course Notes, 12, pp. 79–113.
Pindell, J.L., 1993. Regional synopsis of Gulf of Mexico and Caribbean evolution. In: Pindell, J.L., Perkins, R.F. (Eds.), Transactions of the 13th Annual GCSSEPM Research Conference: Mesozoic and Early Cenozoic Development of the Gulf of Mexico and Caribbean Region, Houston, pp. 251–274.
Pindell, J.L., Barrett, S.F., 1990. Geological evolution of the Caribbean region: a plate tectonic perspective. In: Dengo, G., Case, J.E. (Eds.), The Caribbean Region. Geological Society of America, The Geology of North America, pp. 405–432 (H).
Pindell, J.L., Dewey, J.F., 1982. Permo-Triassic reconstruction of western Pangaea and the evolution of the Gulf of Mexico/Caribbean region. Tectonics 1, 179–211.
Pindell, J.L., Kennan, L., 2001. Kinematic evolution of the Gulf of Mexico and Caribbean. GCSSEPM Foundation 21st Annual Research Conference Transactions, Petroleum Systems of Deep-Water Basins, December 2–5, 2001, pp. 193–220.
Pindell, J.L., Maresch, W.V., Martens, U., Stanek, K.P., 2011. The Greater Antillean Arc: Early Cretaceous origin and proposed relationshiop to Central American subduction mélanges: implications for models of Caribbean evolution. Int. Geol. Rev. 54, 131–143.
Robertson, P., Burke, K., 1989. Evolution of the southern Caribbean plate boundary, vicinity of Trinidad and Tobago. AAPG Bull. 73, 490–509.
Ryan, W.B.F., Carbotte, S.M., Coplan, J.O., O'Hara, S., Melkonian, A., Arko, R., Weissel, R.A., Ferrini, V., Goodwillie, A., Nitsche, F., Bonczkowski, J., Zemsky, R., 2009. Global multi-resolution topography synthesis. Geochem. Geophys. Geosyst. 10, Q03014. http://dx.doi.org/10.1029/2008GC00232.
Schmitt, A.K., Chamberlain, K.R., Swapp, S.M., Mark Harrison, T., 2010. In situ U–Pb dating of micro-baddeleyite by secondary ion mass spectrometry. Chem. Geol. 269, 386–395.
Schuhmacher, M., de Chambost, E., McKeegan, K.D., Mark Harrison, T., Migeon, H., 1993. In situ dating of zircon with the CAMECA ims 1270. In: Benninghoven, A., et al. (Eds.), Secondary Ion Mass Spectrometry SIMS, 9, pp. 919–922.
Seijas, F.J., 1971. Geologia de la regíon de Carúpano. IV Congreso Geologico Venezolano, 5, pp. 1887–1923.
Seton, M., Müller, R.D., Zahirovic, S., Gaina, C., Torsvik, T., Shaphard, G., Talsma, A., Gurnis, M., Turner, M., Maus, S., Chandler, M., 2012. Global continental and oceanic basin reconstructions since 200 Ma. Earth-Sci. Rev. 113, 212–270.
Shaw, D.M., 2005. Trace Elements in Magmas, A Theoretical Treatment. Cambridge University Press, Cambridge (243 pp.).
Sisson, V.B., Ertan, I.E., Avé Lallemant, H.G., 1997. High-pressure (~2000 MPa) kyanite- and glaucophane-bearing pelitic schist and eclogite from Cordillera de la Costa belt, Venezuela. J. Petrol. 38, 65–83.
Snoke, A.W., Rowe, D.W., Yule, J.D., Wadge, G., 2001a. Petrologic and structural history of Tobago, West Indies: a fragment of the accreted Mesozoic oceanic arc of the southern Caribbean. Geol. Soc. Am. Spec. Pap. 354, 56.
Snoke, A.W., Rowe, D.W., Yule, J.D., Wadge, G., 2001b. Geologic map of Tobago, West Indies with explanatory notes. Geological Society of America, Map and Chart Series 087, 1:25 000, 1 sheet.
Speed, R.C., Foland, K.A., 1991. Miocene metamorphism and Neogene tectonics of Northern Range rocks. In: Gillezeau, K.A. (Ed.), Transactions of the Second Geological Conference of the Geological Society of Trinidad and Tobago, Pointe-a-Pierre, Trinidad, pp. 19–20.
Stern, R.J., 2004. Subduction initiation: spontaneous and induced. Earth Planet. Sci. Lett. 226, 275–292.
Sun, S.-S., McDonough, W.F., 1989. Chemical and isotopic systematics of oceanic basalts: implications for mantle composition and processes. In: Saunders, A.D., Norry, M.J. (Eds.), Magmatism in the Ocean Basins. Geological Society of London Special Publication, 42, pp. 313–345.
Tiepolo, M., Botazzi, P., Foley, S.F., Oberti, R., Vannucci, R., Zanetti, A., 2001. Fractionation of Nb and Ta from Zr and Hf at mantle depths: the role of titanian pargasite and kaersutite. J. Petrol. 42, 221–232.
Unger, L.M., Sisson, V.B., Avé Lallemant, H.G., 2005. Geochemical evidence for island-arc origin of the Villa de Cura blueschist belt, Venezuela. In: Avé Lallemant, H.G., Sisson, V.B. (Eds.), Caribbean–South American Plate Interactions, Venezuela. GSA Special Paper, 394, pp. 223–249.
Urbani, F., Rodríguez, J.A., 2004. Atlas Geológico de la Cordillera de la Costa. Ediciones Fundación Geos y Funvisis, U.C.V, Caracas (146 pp.).
Vallejo, C., Spikings, R.A., Luzieux, L., Winkler, W., Chew, D., Page, L., 2006. The early interaction between the Caribbean Plateau and the NW South American Plate. Terra Nova 18, 264–269.

Wadge, G., Macdonald, R., 1985. Cretaceous tholeiites of the northern continental margin of South America: the San Souci Formation of Trinidad. J. Geol. Soc. Lond. 142, 297–308.
Weber, J.C., Dixon, T.H., DeMets, C., Ambeh, W.B., Jansma, P., Mattioli, G., Saleh, J., Sella, G., Bilham, R., Pérez, O., 2001. GPS estimate of relative plate motion between the Caribbean and South American plates, and geologic implications for Trinidad and Venezuela. Geology 29, 75–78.
Weber, M., Cardona, A., Valencia, V., Garcia-Casco, A., Tobón, M., Zapata, S., 2010. U/Pb detrital zircon provenance from Late Cretaceous metamorphic units of the Guajira Peninsula, Colombia: tectonic implications on the collision between the Caribbean arc and the South American margin. J. S. Am. Earth Sci. 29, 805–816.
Wingate, M.T.D., Compston, W., 2000. Crystal orientation effects during ion micro-probe U–Pb analysis of baddeleyite. Chem. Geol. 168, 75–97.
Workman, R.K., Hart, S.R., 2005. Major and trace element composition of the depleted MORB mantle (DMM). Earth Planet. Sci. Lett. 231, 53–72.
Wright, J.E., Wyld, S.J., 2011. Late Cretaceous subduction initiation on the southern margin of the Caribbean plateau: one great arc of the Caribbean or three? Geosphere 7, 468–493.